



University of
Southern
Queensland

**THE COLOUR ANALYSIS OF METEORS USING THE
DESERT FIREBALL NETWORK**

A Thesis Submitted by

Christopher Johnson,
BSc. with Hons.

For the Award of

Master of Science (Research)

2023

ABSTRACT

Meteors have long been studied to determine their origins, whether it be the initial curiosity of ‘What is this bright light streaking across the sky?’, or where these chunks of celestial rocks come from in our Solar system. Colour analysis of meteors has been previously attempted with limited results. Differentiating meteors by colour alone enables efficient automated surveys that help provide a link between meteoroids and meteorites. Currently, there is promising, but limited knowledge regarding the spectra of meteors, with several small studies performed. These studies are hampered by the difficulties of gaining meteor spectra due to their serendipitous nature, and the narrow field of view of current spectrographic instruments. Using photometry, which measures the brightness in a particular colour, to study these events leads to greater accessibility, but a lower accuracy. This can be offset by the larger number of observations possible with a photometric setup. With access to the Desert Fireball Network’s archival data, I have undertaken a pilot study to assess the viability of a large-scale study of meteor colour to detect noticeable colour variations or consistent trends within RGB observations. Through an initial study of the data, I found that colour-indices at a fixed altitude of 75 km reveals a relationship between the colour-index and the initial velocity of an incoming fireball, which is congruent with previous literature. This could allow colour to be used as a proxy for velocity if velocity data is unavailable, or potentially allow shower associations to be proposed or confirmed from a single camera observation. Given the small nature of this data set and the compact time frame in which the data was observed, along with the annual nature of meteor showers, further investigation with the complete DFN dataset is required to confirm if these results are consistent throughout the complete data set.

CERTIFICATION OF THESIS

I Christopher Johnson declare that the Thesis entitled *The Colour Analysis of Meteors Using the Desert Fireball Network* is not more than 100,000 words in length including quotes and exclusive of tables, figures, appendices, bibliography, references, and footnotes. The thesis contains no material that has been submitted previously, in whole or in part, for the award of any other academic degree or diploma. Except where otherwise indicated, this thesis is my own work.

Date: 7 April 2023

Endorsed by:

Professor Jonti Horner
Principal Supervisor

Dr Eleanor Sansom
Associate Supervisor

Associate Professor Duncan Wright
Associate Supervisor

Professor Brad Carter
Associate Supervisor

Student and supervisors signatures of endorsement are held at the University.

LIST OF CONTRIBUTIONS FROM PUBLICATION CO-AUTHORS

This section details contributions by the various authors for each of the papers presented in Chapter 3 of this thesis by publication.

Author	Percent Contribution	Tasks Performed
Christopher J. Todd	75	Original draft, data analysis, data visualisation
E. K. Sansom J. Horner H. A. R. Devillepoix M. C. Towner M. Cupak B. Carter D. Wright	25	Drafting, discussions, editing, writing suggestions, coding help, visualisation thoughts

ACKNOWLEDGEMENTS

I would like to thank my supervisors and the University of Southern Queensland for giving me the opportunity to study in a field of research that has renewed my passion for space and knowledge. I'd like to thank my supervisory team: Professor Jonti Horner, Dr. Ellie Sansom, Associate Professor Duncan Wright, Professor Brad Carter, Dr. Hadrien Devillepoix, Dr. Martin Towner, and Martin Cupak. You have all helped me throughout this journey and I wouldn't have been able to complete this research without you. Hadrien, Martin, and Martin you've helped me understand the DFN system so much, I really appreciate all the guidance and coding help with the DFN python suite and my own code. Thank you, Duncan, for the help with the camera deployment, and thank you, Brad, for always offering helpful and insightful words. Thank you all so much for all the comments and for sticking with me through the countless iteration of my paper.

I would like to thank my primary supervisor, Jonti, for everything you have done for me throughout this process. Whether it be driving to a potential camera site or the seemingly endless edits on my writing this would not have been possible without your input. I would like to thank my secondary supervisor Ellie. This project is awesome to work on and I am so glad I got to meet you in person at the ASRC. Thank you so much for all the science chats, the coding help, and everything else you've done, including contributing to the endless edits.

As always I could not do this without the support of my family, especially my parents. It's been a rough few years, and I am so glad that we all made it to the end of this chapter. A special thanks to my partner Niki, I'm so happy you have come into my life in the past year and I would not have gotten through it half as well as I have without you.

To my friends, you are all like my extended family. I really appreciate the support you've

shown me; reading drafts, getting coffee, talking trash, games nights, dinners, writing, and coding help, the list is endless. Thank you for everything you have done and continue to do for me.

This research is supported by the Australian Research Council through the Linkage Infrastructure, Equipment, and Facilities program (LE170100106). The DFN receives institutional support from Curtin University and uses the computing facilities of the Pawsey supercomputing center. The DFN team would like to thank the people hosting the observatories and the original custodians of these lands, paying respects to elders; past, present, and emerging.

TABLE OF CONTENTS

ABSTRACT	i
CERTIFICATION OF THESIS	ii
LIST OF CONTRIBUTIONS FROM PUBLICATION CO-AUTHORS	iii
ACKNOWLEDGEMENTS	iv
TABLE OF CONTENTS	vi
LIST OF FIGURES	viii
1 INTRODUCTION	1
1.1 Meteoroids	3
1.1.1 <i>Nomenclature</i>	3
1.1.2 <i>Taxonomy</i>	5
1.2 The Spectra	7
1.2.1 <i>Spectral taxonomy</i>	10
1.3 Alternative methods	11
1.4 Limitations	15
1.5 Velocity relation	18
2 DESERT FIREBALL NETWORK SETUP	20
2.1 The hardware and data structure	21
2.1.1 <i>The automatic detection of fireballs</i>	22
2.1.2 <i>Colour extraction</i>	27

2.1.3	<i>Fireball trajectory determination</i>	30
3	PAPER 1 - COLOUR ANALYSIS OF METEORS USING THE DESERT FIREBALL NETWORK	32
3.1	Submitted paper	32
3.2	Abstract	33
3.3	Associated presentations	46
3.3.1	<i>September 2022, Australian Space Research Conference - oral presen- tation</i>	46
4	ANALYSIS AND DISCUSSION	47
4.1	Understanding the data	47
4.2	Colour-indices	49
5	QUEENSLAND NETWORK DEPLOYMENT AND CONCLUSIONS	54
5.1	Eastern network update	54
5.2	Conclusions	55

LIST OF FIGURES

(Excluding publications included in Chapter 3)

1.1	Final stages of ‘life’ for a meteoroid. It can be seen that as a meteoroid enters the upper atmosphere it undergoes a preheating phase before ablation begins in the bright flight phase. As the bright flight phase begins, the meteor will be categorised into one of the three categories on the left (meteor, fireball, or bolide), depending on the resulting interaction between the meteoroid and the atmosphere. If the meteor is not completely dissolved by the ablation process it enters a dark flight phase, reaches the ground and is called a meteorite. This figure is used with permission from Sansom (2016).	4
1.2	The classification structure of meteorites, based upon research presented by Weisberg et al. (2006). The hierarchy of this structure can be seen on the left of the figure, noting that some groups are defined further into subgroups. It can be seen that chondrites consist of only stony meteorites, which is indicative of the nature and history of their parent bodies. Primitive achondrites consist of both stony and iron-type meteorites, while achondrites have examples of all three different types in their classification system. Figure courtesy of Wikipedia/Tobias1984 (2012).	8

- 1.3 This figure shows examples of photometric and spectroscopic spectra. **Left:** The relative transmission can be seen for each filter $[g,r,i,z,Y]$. For each of these filters, a single value is given and photometry calculations can be computed. Figure courtesy of Abbott et al. (2018). **Right:** This is an example spectrum from the SDSS data release 7, the exact candidate can be seen in the legend in the top right. It can be easily seen that there could be far more information immediately gleaned with the CIV, CIII, and MgII features clearly visible. All the features seen on the spectrum would be absorbed into one of the five filters seen in the left panel, resulting in the loss of specific information about the target. For the purpose of this research the shape of the bandpasses (individual filters) is not important, for further discussion on this topic see: Kalmbach et al. (2020). Figure courtesy of Guo and Gu (2014). 9
- 1.4 From this figure a logarithmic layout of the Solar system can be seen. The asteroids mentioned previously (Itokawa, Ryugu, and Bennu) for which samples have been returned to Earth, orbit the Sun between Earth and Mars. The main asteroid belt can be seen between Mars and Jupiter, approximately 3 astronomical units (au) from the Sun. Jovian and Neptunian Trojans can be found orbiting in the same space that the planets from which they are named inhabit, at ≈ 5 and ≈ 30 au, respectively. Trans-Neptunian and Edgeworth-Kuiper belt objects can be seen between 35 and 60 au, this includes several dwarf planets, such as Pluto. Voyager 1 and 2 are currently in interstellar space (≈ 155 and 130 au respectively), having crossed into the Heliosheath [turbulent layer where the solar wind stops and interstellar winds start to take over] in December 2004 and August 2007, respectively. Both probes are currently in the outer half of the yellow band, starting at ≈ 85 au. The Oort cloud, home to much of the Solar system's cometary material is not pictured in this image as it is thought to range from as close as 2000 au and as far as 200,000 au (Morbidelli, 2005). Figure courtesy of Frohn (2017) 14

2.1	Left: Billa Kalina DFN camera installation, complete with solar panel and antenna. The sunshield of the DFN observatory can be seen camouflaged into the horizon atop the ground-based stand. Fencing can be seen surrounding the observatory to add extra protection (from livestock as several cameras are in farming paddocks) or visibility/awareness depending on what is necessary. Right: Billa Kalina DFN camera installation from the reverse angle, which shows the battery and power converter underneath the solar panel and the DFN observation housing on the stand. [Photos courtesy of the DFN wiki, taken by Martin Cupak]	21
2.2	These images are of a typical Global Fireball Observatory (GFO) rooftop installation. Left: Camera housing internals. From top right in a clockwise direction, you can see the camera, hard drive storage, PCBs, and video camera. Right: Housing installation at Mt. Kent observatory, currently awaiting network connection to start operations and collect data. [Photographs taken by the author.]	23
2.3	Left: DN151203_01 fireball observation from the Etadunna observatory on 3 December 2015. Here the de Bruijn sequence encoding is clearly visible within the image as dashes. Right: DN151212_03 fireball observation from 12 December 2015, again from the Etadunna observatory. This is the entire frame using a fish-eye lens from a large fireball event. The de Bruijn encoding is not as obvious as the adjacent image, this is because sensors have been saturated by the brightness of the event. This means there is too much light observed in that pixel, and it begins to bleed into the adjacent pixels causing smears.	24
2.4	This figure shows an example of an image that suffers from meteorological interference. Luckily the meteor observed was in a tile far enough away from the Moon that it was still able to be analysed. The image was taken from the Mundrabilla observatory in Western Australia, on the 19 th of December 2015.	25
2.5	Here the plot on the left shows the two points in the x y space, while the plot on the right shows these points represented in the Hough space. The intersection of these lines in the Hough space (in the right-hand graph) corresponds to the line that passes through both of these points in the x y space (the left-hand graph). Image borrowed from Lee (2020).	26

2.6	Left:	This is a visual representation of the SLLS method. The line of best fit can be seen to pass through the middle of the points and would give the trajectory of the meteor in its bright flight phase.	Right:	Shows how the method of planes is used to construct the trajectory of the meteor in its bright flight phase. A plane is drawn between the observing station and the start and end points of the meteors bright flight phase. This is done from all stations that observe the given meteor and the trajectory is calculated to be the intersection of the planes.	31
4.1		The left panel shows the apparent magnitude for the duration of the fireball's bright flight. The right panel shows a plot of the colour-indices. The small gap in the centre of the colour-index plot is due to the saturation of the green colour channel, which can be seen represented by crosses in the left panel, indicating the sensor was saturated by the amount of light in that colour band. This figure is produced from data gained from a fireball observed on the 28 th of December 2015, from the Wooleen observatory in Western Australia.			48
4.2		This figure shows an example of all observations from a single event in one graph. In the left panel, the apparent magnitude of the RGB colour channels can be seen. Each station is represented by a different marker, with five in total for this event. Data from Mulgathing (circle), Ingomar (inverted triangle), Baton (plus), Mount Barry (star), and William Creek (square) can be seen, with the colours representing the colour channel of the data (red, green, or blue). In the right panel, the available colour-indices can be seen (B-R, B-G, and G-R), using the same markers for each observation. This figure was produced with data gathered from the five observatories listed in South Australia from a fireball on the 5 th of November 2015.			49

- 4.3 Shows the initial equatorial positions of available fireballs with the colour-bars indicating the average colour-index (from left to right: B-R, B-G, and G-R) of the entire bright flight phase. From Figure 4.3, it can be noted that some fireballs fall outside of the quoted range, these instances are represented as the colours at the extremities of the colourbars. Figure ?? can be used as a reference to assist in locating specific showers. In this figure shower members are plotted as diamonds, while the crosses represent the sporadic data set. 52
- 4.4 Shows the initial equatorial position of available fireballs which pass through an altitude of 75km, with the colourbar indicating the colour-index (from left to right: B-R, B-G, and G-R) at this altitude. Fireballs with a colour-index outside the colourbar range are represented by the extremity colours of the associated colourbar. Figure ?? can be used as a reference to assist in locating specific showers. As with Figure 4.3 shower members are plotted as diamonds, while the crosses represent the sporadic data set. 53

1

INTRODUCTION

THROUGHOUT history there have been countless descriptions of objects falling from the heavens, some thought to be harbingers of death, destruction, and the end of days. The great meteor storm of 1833, was described by some as the night ‘the stars descended like snowfall to Earth’ (Thompson Sr., 2012). When it was in fact a Leonid shower outburst, caused by a more compact, higher density debris field from a recent perihelion outgassing (Asher, 1999) of parent comet 55P/Tempel-Tuttle (Yeomans, 1981; Yeomans et al., 1996; Asher et al., 1999). Over the course of many cometary orbits, these compact, high density debris fields distribute meteoroids throughout the orbital path of the meteor stream, adding to or replenishing the stream for future passes through Earth’s orbit. These shards of debris, not only result in stunning visual displays in the Earth’s atmosphere, but some are strong enough and large enough that they make it to the surface of Earth. It is these celestial shards that can be a stepping stone to un-

derstanding the conditions and processes undergone in the Solar system at the time of formation.

While the observations of impacting celestial objects could be important for the survival of life on Earth, all but a handful of impactors in the lifetime of Earth have had little, if any impact on the day-to-day life of its inhabitants. The majority of asteroidal and cometary material fails to reach the surface of our planet (Love and Brownlee, 1993; Bland and Artemieva, 2006; Plane, 2012), which makes observing and studying these falls an interesting and helpful field. The study of this fallen material can give insights into the formation of planets and our Solar system from the earliest epochs in our celestial backyard.

With the Earth's growing population and rise of technology, recordings of fireball sightings have become ever more common. However, whilst such sightings attest to the frequency of such events worldwide, such solitary observations are often of little use scientifically, beyond simply telling us that an event has happened in a certain area. To learn more, a concerted program of observation is needed. Many different disciplines assist in sifting through the wealth of knowledge that can be gained from a meteorite. There is a vast amount of scientific disciplines involved in the study of meteoroids. The fields of geology, petrology, and biology allow information to be gained from the meteorites found on the Earth's surface (Jenniskens and Stenbaek-Nielsen, 2004; Weisberg et al., 2006; Hutchison, 2007; Osinski et al., 2020). Climatology and chemistry help model spectra and flight patterns of meteors as they traverse the atmosphere (Trigo-Rodríguez, 2014; Sansom et al., 2015, 2017). While seismologists and astronomers study the initial asteroids and comets as they orbit the Solar system as well as the impacts of meteorites here on Earth and other planets, or moons¹ (Weisberg et al., 2006; Garcia et al., 2022). These disciplines and many others allow this

¹Note that meteors that impact planets or moons without atmospheres should not be called meteors, but just impacts as they are not affected by an atmosphere and therefore always hit the surface (Tomko and Neslušan, 2023).

plethora of information to be recorded and analysed in the hope of unpacking the origins of the Solar system and the tiny building blocks of its formation.

1.1 METEOROIDS

1.1.1 *NOMENCLATURE*

The term “meteoroids” is a general catchall to describe small pieces of dust and debris floating around the Solar system, smaller than the easily detectable objects from Earth (such as asteroids, comets, dwarf planets, and planets; FI, 2017; Richardson, 2021). Since the Solar system is littered with debris, our planet experiences a constant rain of meteoroids as it moves in its orbit around the Sun. Meteoroids are smallish rocks that may have originated from larger asteroids or comets, through collisions in the case of asteroids or the natural ejection of cometary material as a comet orbits close to the Sun. As meteoroids enter the Earth’s atmosphere (or that of any other planet) and decelerate, they become visible due to a bright heating phenomenon and are renamed meteors, more commonly known as shooting stars or fireballs (for the brightest observations). Should a meteor reach the Earth’s surface intact, then the fallen object is termed a meteorite, which can be designated as either a fall or a find. Meteorites that have been designated as falls, have associated data from their journey through the atmosphere, resulting in an expedition to aid in their recovery. Whereas, finds do not have an associated fireball event and have been located in the environment in which they fell (examples of both falls and finds can be found here; Grossman, 2005). As a result, finds have been exposed to terrestrial conditions and weathering for an unknown period of time, increasing the likelihood that they have been significantly altered since their arrival on our planet. For this reason, meteorites (falls) with known observations, and whose recovery happened rapidly thereafter, are often considered to be of scientific value, since they represent pristine samples of extraterrestrial objects.

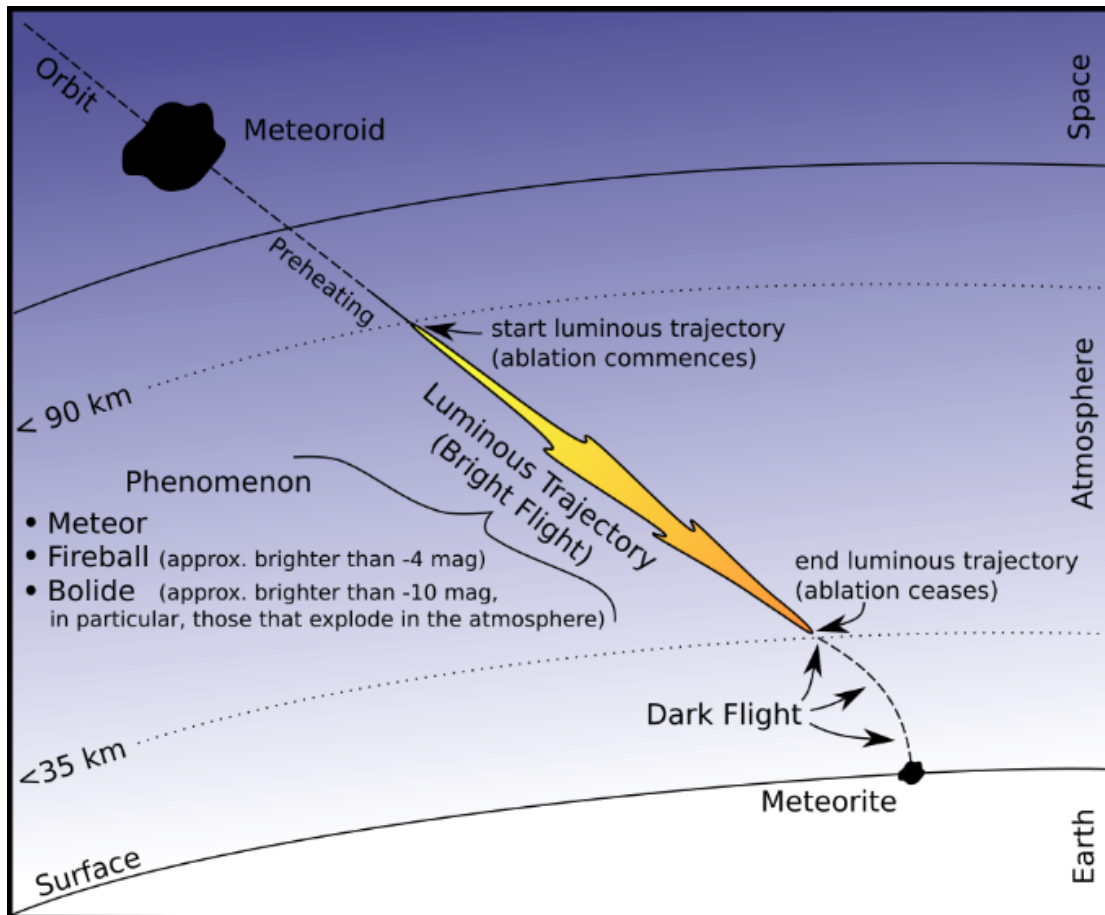


Figure 1.1: Final stages of 'life' for a meteoroid. It can be seen that as a meteoroid enters the upper atmosphere it undergoes a preheating phase before ablation begins in the bright flight phase. As the bright flight phase begins, the meteor will be categorised into one of the three categories on the left (meteor, fireball, or bolide), depending on the resulting interaction between the meteoroid and the atmosphere. If the meteor is not completely dissolved by the ablation process it enters a dark flight phase, reaches the ground and is called a meteorite. This figure is used with permission from Sansom (2016).

Most meteors are just called meteors, but some can be known by more specific names. Depending on size and brightness, specific meteors can be classified as Brownlee particles, fireballs, or bolides. Brownlee particles (or micrometeorites) are dust particles that enter the atmosphere and make it to the Earth's surface intact (Ganapathy and Brownlee, 1979). A fireball is a meteor that is visually brighter than Venus, which has an apparent magnitude between -3 to -5 (depending on Venus's phase and distance from Earth; Redfern, 2020; Richardson, 2021), and bolide is a fireball that explodes in the Earth's atmosphere (Richardson, 2021). This explosion is caused by a process known as ablation. The ablation process is the degradation of a meteor due to aerodynamic pressures caused by factors exerted on the meteor by the Earth's atmosphere, such as drag, heat, and pressure. In most cases, the ablation process will dissolve the incoming meteor. In a small fraction of cases ablation results in the meteor breaking up mid-air, which greatly decreases the chances of finding the subsequent fractions (see Figure 1.1 for a visual explanation). Brownlee particles do not undergo ablation, they are too small and are slowed down by the Earth's outer atmosphere prior to reaching altitudes where high entry velocities would cause ablation (this is why they reach the Earth's surface intact; Ganapathy and Brownlee, 1979).

1.1.2 *TAXONOMY*

Meteoroids represent a vast sample of objects scattered throughout the Solar system, despite being thought originally to come from a single dominant source (Jenniskens, 2006). The composition of individual meteorites is a reflection of their origin and therefore can tell us a great deal about the Solar system's formation and evolution, along with the history of their parent bodies. The Solar system formed from a vast, dense cloud of gas and dust. As this dust and gas began to collapse and form the Sun, it left behind a small amount of material in the planetary plane which further differentiated itself into the planets and other objects we currently see in the Solar system. Asteroids and comets are the shards of debris left behind by the formation of the plan-

etary bodies and are the last remnants of this accretion process.

In a broad sense, there are two main types of meteorites; chondrites and achondrites, with a third type that is a hybrid of both of these main types, primitive achondrites (see Figure 1.2). Chondrites are said to be undifferentiated and likely originate from collisions between asteroids that have not grown to a large enough size to possess a molten core. These collisions result in smaller pieces fracturing off and being sent on new trajectories. Achondrites are commonly referred to as differentiated, which means that they are fragments of objects that grew to a sufficient size in their youth (typically larger than a few hundred kilometres) to have a core temperature hot enough to become molten. This allows denser material to sink to the centre, while less dense material would rise to the surface, leading to a structure that can be found in the terrestrial planets, consisting of a core, mantle, and crust.

Achondrites are likely to have originated from these larger asteroids like Vesta (Binzel and Xu, 1993; McCord et al., 1970), but some have been found to possess Martian (McSween, 2001; Nyquist et al., 2001) or Lunar (Papike et al., 2018) origins. Such meteorites were likely produced by large impacts on those bodies, which have ejected material intact into space, and sent them on a collision course with Earth (Jr. and Treiman, 2018; Papike, 2018). The third major type of meteorite can be classified as primitive achondrites. These exhibit properties from both chondrites and achondrites, more technically they possess the appearance of achondrites, but their chemical makeup closely resembles that of chondrites (Weisberg et al., 2006).

The three types of meteorites mentioned previously are also known as the 'order' in the meteorite classification hierarchy, a visual representation of which can be seen in Figure 1.2. In this hierarchy, the order of the meteorites is the highest tier of categorisation, with each order being further categorised by class, clan, group, and subgroup. These categories increase in specificity for each level, with each being more specific than the last, with differing criteria used for chondrites and achondrites (Weisberg et al., 2006).

Meteorites are sometimes loosely classified into three broad categories; stones, irons, and stony-irons. As seen in Figure 1.2, chondrites consist solely of stony meteorites, which is consistent with their origins. Achondrites, by contrast, have examples of all of these categories, with the primitive achondrites being composed of stones and irons. The more specific group classifications (such as groups and subgroups) are distinguished by chemical abundances and ratios (common refractory elements like Vanadium, Chromium, Manganese, Osmium, and Iridium; Snead et al., 2019, and the ratios of O-isotopes), petrology (formation conditions), and mineralogy (sizes and shapes of chondrules; Weisberg et al., 2006). For chondrite classification, CI chondrites (seen in the row labeled group on the far left of Figure 1.2) possess the closest chemical abundance to the Sun, and they are often used to group other chondrites into their classes and clans. This is done by comparing the abundances of lithophile elements. Lithophile elements are known to combine readily with oxygen, and would typically be expected to remain close to a planet's surface during the process of its differentiation. For Carbonaceous chondrites, the refractory lithophile elements are more abundant than in CI chondrites (refractory elements have a condensation temperature between 1500-1700K). A more detailed discussion and history of meteorite classification can be in Mittlefehldt (2003); Krot et al. (2013); Brearley and Jones (2019); Mittlefehldt et al. (2019) and the references therein, as further discussion is outside the scope of this thesis.

1.2 THE SPECTRA

The electromagnetic spectrum is one of the greatest tools in the tool belt of all astronomical researchers. From radio waves (low energy, $\geq 10^{-2}$ m long) being used to discover the cosmic microwave background (CMB; Penzias and Wilson, 1965), to gamma rays being used to aid in the study of pulsars, magnetars, and quasars (high en-

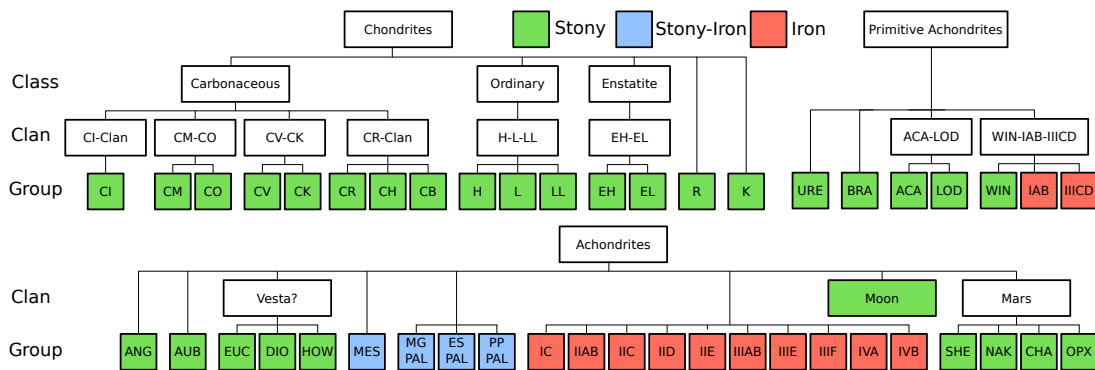


Figure 1.2: The classification structure of meteorites, based upon research presented by Weisberg et al. (2006). The hierarchy of this structure can be seen on the left of the figure, noting that some groups are defined further into subgroups. It can be seen that chondrites consist of only stony meteorites, which is indicative of the nature and history of their parent bodies. Primitive achondrites consist of both stony and iron-type meteorites, while achondrites have examples of all three different types in their classification system. Figure courtesy of Wikipedia/Tobias1984 (2012).

ergy, 10^{-12} m short; Hobbs et al., 2004). The human eye can only perceive a small fraction of the total spectrum, known as the visible spectrum, which ranges approximately from 400-700nm ($4 - 7 \times 10^{-7}$ m). Spectra can be used in a variety of ways including; spectroscopy to find the chemical composition of sources, to using the Doppler shift to find the line of sight velocity of stars or galaxies.

The two types of astronomical surveys are photometric and spectroscopic. Photometric surveys like the Dark Energy Survey (DES; Abbott et al., 2018) take long exposure images and give a flat field of view. From these images, each galaxy or star is analysed using a specific set of filters which dependent on the type of survey, in the case of DES, the filters; g , r , i , z , Y (as seen in the left panel of Figure 1.3). In contrast, a spectroscopic survey, like the Sloan Digital Sky Survey (SDSS; Eisenstein et al., 2001) or the GALactic Archaeology with Hermes Survey (GALAH; Buder et al., 2021) will take a full spectrum from each of the desired targets (an example of such a spectrum can be seen in the right panel of Figure 1.3). For each of the filters in the photometric survey (Figure 1.3 left) a single value is registered instead of the continuous values seen in the spectroscopic counterpart (Figure 1.3 right).

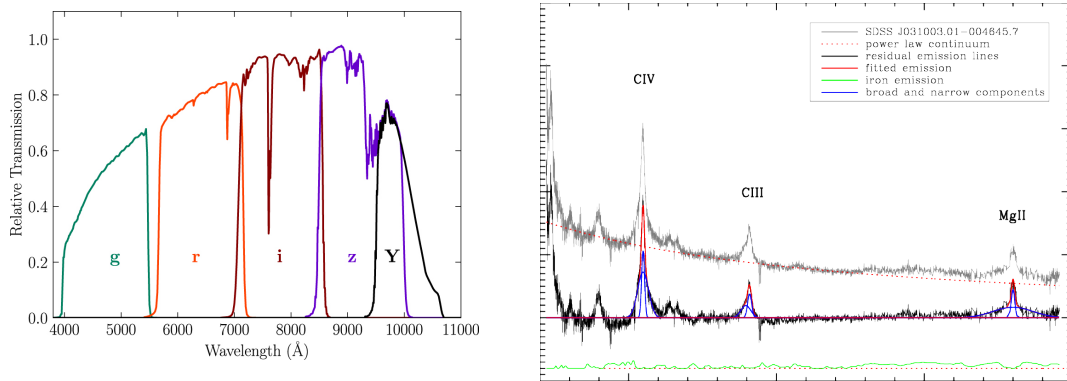


Figure 1.3: This figure shows examples of photometric and spectroscopic spectra. **Left:** The relative transmission can be seen for each filter [g, r, i, z, Y]. For each of these filters, a single value is given and photometry calculations can be computed. Figure courtesy of Abbott et al. (2018). **Right:** This is an example spectrum from the SDSS data release 7, the exact candidate can be seen in the legend in the top right. It can be easily seen that there could be far more information immediately gleaned with the CIV, CIII, and MgII features clearly visible. All the features seen on the spectrum would be absorbed into one of the five filters seen in the left panel, resulting in the loss of specific information about the target. For the purpose of this research the shape of the bandpasses (individual filters) is not important, for further discussion on this topic see: Kalmbach et al. (2020). Figure courtesy of Guo and Gu (2014).

In large continent size camera networks, like DFN (Devillepoix et al., 2020) and FRIPON (Colas, F. et al., 2020), it is not feasible to use spectroscopy as part of the data collection, due to the extra cost, power, and data processing needed (Howie, Paxman, Bland, Towner, Cupak, Sansom and Devillepoix, 2017). These large systems use DSLR (digital single-lens reflex) cameras which possess a Bayer colour filter. The Bayer filter has alternative columns and rows of red-green and blue-green sensors, this is to closely match the process in the human eye (Bayer, 1976). This process is more similar to photometry, in that the magnitude from each sensor in the camera (RGB) can be thought of as the magnitude in each filter measured and used to calculate the absolute magnitude of the meteor (see Section 2.1.2 for a more detailed discussion of this process).

As spectroscopy is not an option, the more intricate analysis of chemical abundances, from such studies as Borovicka (1993) and Vojáček et al. (2015a), among others, is not possible. An analysis of meteor colour using RGB has been touched on previously,

by Moorhead and Kingery (2020). This was in conjunction with spectra data which adds further ability to draw conclusions from the results. The results were inconclusive, with most categories indistinguishable from one another, with only iron meteors exhibiting categorisable differences. However, this does show the viability of using only colour to analysis and categorise meteors.

1.2.1 *SPECTRAL TAXONOMY*

With the advancement of optical technology, it is becoming increasingly easy to generate and analyse spectra of asteroids, with telescopes such as the one found at the Vera C. Rubin Observatory. Several attempts at classification of asteroids have been made, most notably by Tholen (1984) and Bus (1999), both using principal component analysis to group asteroids based on colour-indices and the shape of their spectra.

Before Tholen (1984), attempts were made to classify asteroids using their spectra and colours with limited success. This was mainly due to the smaller sample sizes available at the time, some smaller than 50 (Tholen, 1984). Tholen (1984) was the first (and largest, at the time) study of its kind to use principal component analysis to classify asteroids. This initial classification consisted of 14 categories based on the shape and slope of the spectra observed. Through the advancement in imaging and spectroscopy techniques Bus (1999) built upon this, and extended this to a 26 category system, using 48 data points along the spectrum compared with 8 in the Tholen (1984) system. Further attempts to extend and consolidate the Bus (1999) system have come through DeMeo et al. (2009). DeMeo et al. (2009) did this by extending the studied spectrum range into the infra-red. DeMeo et al. (2009) use a spectra range of $0.45\text{-}2.45\mu\text{m}$, compared with $0.435\text{-}0.925\mu\text{m}$ and $0.34\text{-}1.04\mu\text{m}$ for Bus (1999) and Tholen (1984), respectively. This allowed for a potential recalibration of the Bus taxonomy to the Bus DeMeo taxonomy system. DeMeo et al. (2009) proposes the elimination of three and an addition of one to the 26 categories present in the Bus system, leaving the

new system with 24 categories. A more in-depth discussion can be found in DeMeo et al. (2009), with a summary of the categories and their features in Table 5 of that text.

While all of this is important for the classification of asteroids, monitoring population numbers, and categorising locations, a much larger and more in-depth study would need to be undertaken to marry up these distinct fields of study. This would involve cross-matching of asteroids, comets, meteors and meteorites to make more detailed conclusions or to calibrate any sort of classification system which could be used with minimal success, as only a small proportion of asteroidal material would fit into all of these categories (asteroid, meteor, and meteorite)². This is also assuming that you have the spectra of meteors as they are travelling through the atmosphere, which DFN does not for various reasons, as outlined in Howie, Paxman, Bland, Towner, Cupak, Sansom and Devillepoix (2017).

1.3 ALTERNATIVE METHODS

With a mass of more than 330,000 times that of the Earth (M_{\oplus}), the Sun is by far the largest object in the Solar system. In contrast, the total mass contained within the planets and other small bodies in the Solar system (within a few tens of astronomical units (au) of the Sun) is estimated at less than 500 M_{\oplus} (with the majority of this mass residing in Jupiter, at $\sim 318 M_{\oplus}$; Horner et al., 2020).

The total amount of mass contained in Solar system objects that have yet to be discovered is much more uncertain, with estimates ranging between $2 \times 10^{-2} M_{\oplus}$ (Vladimirovna Pitjeva and Petrovich Pitjev, 2015) and $6.6 \times 10^4 M_{\oplus}$ (Mendis and Marconi, 1986). This uncertainty is primarily driven by the diversity of opinions on the total mass contained within the Opik-Oort cloud. This also takes into account the suggestions that there

²Discussed further in Section 1.4.

may be undiscovered planet-mass objects lurking in the depths of the Solar system (e.g. Brown et al., 2004; Trujillo and Sheppard, 2014; Volk and Malhotra, 2017; Lykawka and Ito, 2023, among others.).

The majority of known asteroidal and cometary material can be found in reservoirs such as the Asteroid belt, Jovian and Neptunian Trojans, trans-Neptunian objects (including Edgeworth-Kuiper belt), and the Opik-Oort cloud (Carroll and Ostlie, 2007; Horner et al., 2020). Horner et al. (2020) gives a more detailed and complete list of the distribution and size of these populations and a visual of where these objects sit within the Solar system can be seen in Figure 1.4.

This asteroidal and cometary material are remnants left behind from the creation of the Solar system. Studying these objects could be key to further understanding the constituents and processes that were occurring during the early part of the creation of the Solar system. But how do we get a good look at them? Pointing a telescope at them for days and weeks can only tell you so much information and cannot give all the insights required to understand how, where, and when these objects were formed. In reality, this is not a great use of telescope time, given the low reflective qualities of these objects (both albedo and faintness). This type of study is becoming more common with the advancement of telescopes such as the construction of the ground based Vera C. Rubin Observatory (Siraj and Loeb, 2021, 2020; Jones et al., 2016), and the launch of the space based observatory James Webb Space Telescope (JWST, Rigby et al., 2022). These kinds of observations could help with the spectral classification of asteroids, as mentioned in section 1.2.1.

This means there are two options moving forward on studying meteoric material. Either, visiting these objects in space, via sample return missions, or finding and collecting meteorites from the Earth's surface. Efforts have successfully been made in landing on, retrieving, and analysing cometary or asteroidal material in the past. The Japanese *Hayabusa* spacecraft visited 25143 Itokawa (Yoshikawa et al., 2021), *Hayabusa2* visited

162173 Ryugu (Sugita et al., 2020), and the *OSIRIS-REx* NASA mission visited 101955 Bennu and is currently returning to Earth (Dworkin and Osiris-Rex Team, 2017). All of these missions come with a large price tag, but they also give a large amount of data and experience for future endeavours as well as corroboration of knowledge gained from Earth based collection missions. The downside to these missions is that they are only looking at objects within a small volume of our inner Solar system. This is because of the massive time and financial commitment involved in looking further abroad. This can be easily realised when looking at the Voyager missions (NASA, 1981; McNutt et al., 2020), taking more than 10 years to pass by Neptune which is only about 80 percent of the distance to the Edgeworth-Kuiper belt.

Given the length of these missions, this immediately rules out crewed mission to retrieve samples. Even the current missions to inner Solar system locations, such as the *OSIRIS-REx* mission with an expected return in 2023, have taken several years. This is without having larger payloads and engines to accommodate the survival and return of passengers. Such a mission would significantly increase not only the cost of the mission but also the time taken to achieve similar results. These complications lead to the question of whether there are alternative strategies to find information in a timely and cost effective manner.

Like all other objects in the Solar system, the Earth experiences meteoroid impacts. Some of these impacts are large enough to disrupt an eco-system, but most are small enough to not even leave a trace as they have traversed the atmosphere. Between these two extremes fall the meteorites, these provide the ideal means by which scientists can analyse primordial material from the Solar system's youth. But what is the best way to find these objects? The detection of meteors and subsequent locating and study of the resulting meteorite has been a growing field of astronomical science since it began in the late 1930s (Whipple, 1938). Many camera networks have been established across several countries to aid in this scientific pursuit. The Global Fireball Observatory (GFO) collaboration (Devillepoix et al., 2020) and the Fireball Recovery and InterPlanetary

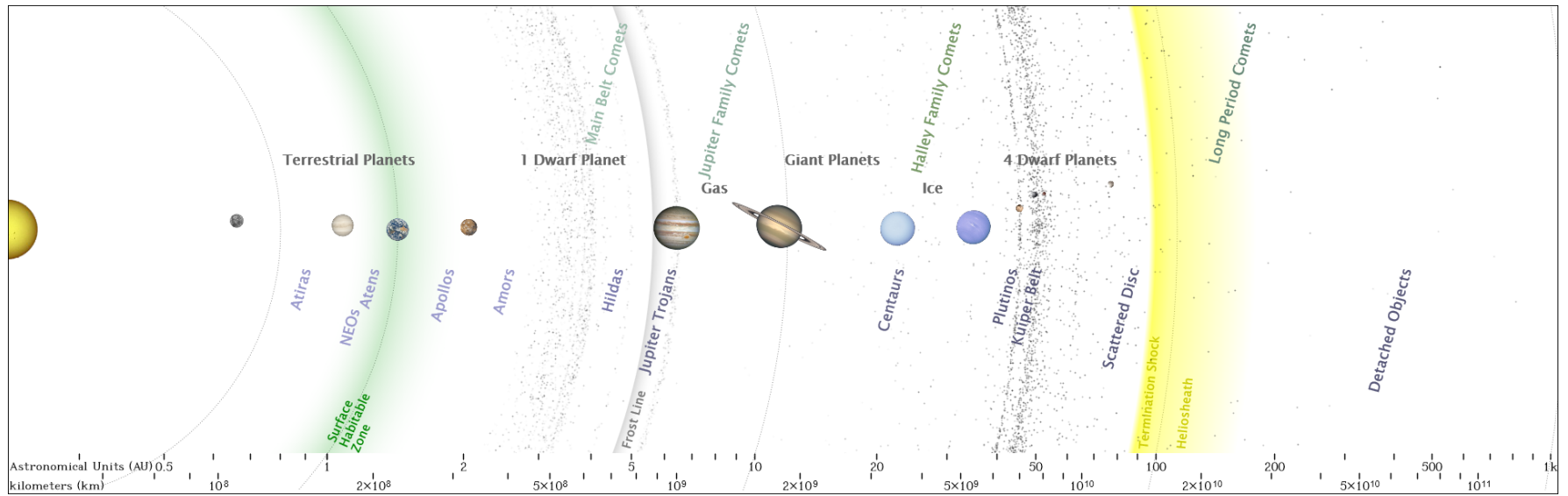


Figure 1.4: From this figure a logarithmic layout of the Solar system can be seen. The asteroids mentioned previously (Itokawa, Ryugu, and Bennu) for which samples have been returned to Earth, orbit the Sun between Earth and Mars. The main asteroid belt can be seen between Mars and Jupiter, approximately 3 astronomical units (au) from the Sun. Jovian and Neptunian Trojans can be found orbiting in the same space that the planets from which they are named inhabit, at ≈ 5 and ≈ 30 au, respectively. Trans-Neptunian and Edgeworth-Kuiper belt objects can be seen between 35 and 60 au, this includes several dwarf planets, such as Pluto. Voyager 1 and 2 are currently in interstellar space (≈ 155 and 130 au respectively), having crossed into the Heliosheath [turbulent layer where the solar wind stops and interstellar winds start to take over] in December 2004 and August 2007, respectively. Both probes are currently in the outer half of the yellow band, starting at ≈ 85 au. The Oort cloud, home to much of the Solar system's cometary material is not pictured in this image as it is thought to range from as close as 2000 au and as far as 200,000 au (Morbidelli, 2005). Figure courtesy of Frohn (2017)

Observation Network (FRIPON) science project (Colas, F. et al., 2020) are two of the biggest endeavours to track and recover meteorites in current times.

The GFO includes networks from Argentina, Australia, Canada, Morocco, the Kingdom of Saudi Arabia, Oman, the United Kingdom, and the United States of America, with over 90 cameras, covering $\approx 5 \times 10^6 \text{km}^2$ (Devillepoix et al., 2020). The majority of these cameras can be found in the Australian outback, which, because of the vast areas of unpopulated space in the interior of the country, is the perfect location to track and recover meteorites. Known as the Desert Fireball Network (DFN), the branches of this network extend across five of the eight states and territories in Australia (Devillepoix et al., 2020). The FRIPON science project includes 150 cameras and 25 radio receivers, the majority of which exist in France and neighbouring countries, with 22 countries in total participating, covering $\approx 1.5 \times 10^6 \text{km}^2$ (Colas, F. et al., 2020).

1.4 LIMITATIONS

A lot is known about the composition of asteroids from spectral analysis seen in Tholen (1984); Bus (1999); DeMeo et al. (2009) along with others who have continued and built upon this work. A far smaller amount is known about the spectra of meteors (see: Borovička et al. (2005); Vojáček et al. (2015*b*), among others), due to the difficulty of taking meteor spectra. The most reliable way to gain high resolution spectra of meteors is to position a spectrometer directly facing the radiant of a known meteor shower (Ceplecha et al., 1998). This is due to the narrow field of view of such instruments.

Due to the restrictions and design challenges of the DFN, spectroscopic analysis of meteors is not an option, this is discussed further in Howie, Paxman, Bland, Towner, Cupak, Sansom and Devillepoix (2017). Instead, the colour channels of DSLR cam-

eras are used as a sort of photometric analysis, or very low resolution spectra. A total amount of flux for a particular channel (in this case R, G, or B) is found and the colour in each channel is analysed. The flux received from the target sums together and contributes to the total flux found in each channel. This type of analysis eliminates the ability to identify the ratios or individual constituents present in a meteor's spectra. However, this method can still offer potential insights into the bulk properties present in different individual meteors, as seen by results presented in Moorhead and Kingery (2020) or potentially meteor streams.

Ideally, it would be possible to determine the composition and shower association of a given meteor based solely on its colour, velocity, and potentially the time of year at which it was observed. However, to reach this level of accuracy, we would first need to have gathered a large amount of prior information on meteors in general, from many years of observations. Theoretically, with enough background information, a classification system could be possible – but it is obvious, at the moment, that we are a long way from having enough data to manage this. To truly understand the complexities involved, I outline below the major pieces of information needed to create a classification system capable of predicting the composition and shower association of a given meteor.

To create the models that would be needed for this hypothetical future classification system you would need to observe a meteor in the bright flight phase and gain the spectroscopic and photometric fall data. This becomes problematic given that collaborations tend to focus on either photometric or spectroscopic measurements, not both. This is due to the different challenges associated with each measurement type. You would then need to be able to recover the meteorite mostly intact. This is to confirm the composition and compare the colours seen in the bright flight phase. This is difficult as most meteorite samples originate from a sporadic origin, meaning they do not have an associated shower. This is because shower material is typically from weaker cometary material, which does not often survive the dynamic pressures that it

is exposed to upon entry.

From this data, you would need to be able to discern the orbital information, to better understand potential parent bodies and/or points of origin in the Solar system of this particular meteoroid. However, due to the highly chaotic nature of orbital evolution and orbital dynamics, there are limits to the long-term dynamical history of pre-atmospheric orbits able to be determined. Lastly, pre-existing knowledge of the parent body would need to be accurate. However, many meteor shower origins are still currently under debate, and some studies can only offer ‘best guesses’ with the currently available information. Finally, having amassed all of this data and information you would be able to build a repository associating key features with variations in colour allowing composition and shower associations to be suggested from colour and velocity.

This is an amount of information that is unattainable with current techniques and technology, even for the most complete meteorites in worldwide collections. Only about 50 of the ~70,000 meteorites possess pre-atmospheric orbital data (Grossman, 2005; Meier, 2017). To further complicate this, natural variation within the spectrum of meteors from the same shower adds an extra layer of difficulty to this situation. An example of this can be seen in Vojáček et al. (2015*b*), with two meteors from the same shower possessing vastly different spectrum. Spectra from meteors could also be different from year to year, as solar radiation has been known to deplete populations of their more volatile chemicals (Trigo-Rodríguez and Llorca, 2007; Čapek and Borovička, 2009). This too would alter the spectrum measured from meteors as they traverse the atmosphere on a year to year basis.

The work presented in this thesis hopes to bridge to the gap in the knowledge found in this area of research. Due to the difficulties in gaining meteor spectra, it is hoped that a photometric equivalent, in this case, colour analysis, can be used with a large enough data set to assist and further categorise meteors. Variations in RGB colour

could be used to:

1. more efficiently differentiate between known shower members and sporadic meteors,
2. identify meteors that share a common origin but have been moved onto orbits greatly different to their siblings (potential shower members, that have strayed from their orbital path and consequently been designated as sporadic),
3. tighten constraints on a meteor's physical parameters, allowing shower associations to be considered or potentially confirmed from single camera observations.

1.5 VELOCITY RELATION

It has been well established by several studies (e.g. Ceplecha, 1959; Davis, 1963; Hajduková, 1967, among others), that there is a relationship between meteor brightness and colour-index. Jacchia (1957), tried to take this one step further, by analysing the colour-index in relation to meteor velocity. The colour-index of these meteors was measured in a much different way due to the cost and availability of colour photographing equipment. Using a special film which was sensitive to blue light, and naked eye observations, Jacchia (1957) was able to construct a colour-index comparable to the modern B-V (blue – visual) colour-index. From the data collected, 315 meteors were analysed by first splitting the meteors into velocity groups (slow, <22 km/s; medium, $22 < v < 40$ km/s; fast, >40 km/s), then, binning the meteors by colour-index and counting the number in the resulting bins. Through this process, Jacchia (1957) concluded there was no association between colour-index and meteor velocity.

Hajdukova (1974) instead proposed that the conclusion reached in Jacchia (1957) was incorrect as they did not take into account the opposing directions of the dependencies of velocity and brightness on the colour of a meteor. Using the same sample, Hajdukova (1974) was able to show after correcting for this error, that meteor colour

is dependent upon the velocity of the incoming meteor. Figure 4 of Hajdukova (1974) shows this correlation. The paper finds, meteors with a lower velocity are bluer at a rate between 12 and 16 mmag per km/s. Meaning that over the range of velocities presented in Hajdukova (1974), from ~ 14 to ~ 70 km/s, the magnitude should differ by between 0.672 to 0.896 magnitudes.

With the advancement and greater cost-effectiveness of photographic equipment, the DFN has been able to make large strides in capturing large numbers of fireballs in colour on film. This means through analysis, discussed further and in more detail in Chapter 2, several different colour-indices of incoming fireballs can be calculated. Given this advancement in photographic equipment the colour-indices calculated in this work are different to the ones used in Jacchia (1957) and Hajdukova (1974), or others of the time. This means we must use the most similar to be able to effectively compare this work with previous literature (see Section 2.1.2 in the next chapter for a discussion).

2

DESERT FIREBALL NETWORK SETUP

A. S. Herschel was the first to study meteor spectra in the 1860's (early history of meteors discussed in; Millman, 1937). Since this time efforts have been made to continue and build upon this work. The Desert Fireball Network (DFN; Devillepoix et al., 2020) and the Fireball Recovery and InterPlanetary Observation Network (FRIPON; Colas, F. et al., 2020) are two of the collaborations to study these phenomena, with DFN being the only network currently to record in full colour. In this chapter, I present an overview of the DFN and describe how the data is collected and processed.



Figure 2.1: Left: Billa Kalina DFN camera installation, complete with solar panel and antenna. The sunshield of the DFN observatory can be seen camouflaged into the horizon atop the ground-based stand. Fencing can be seen surrounding the observatory to add extra protection (from livestock as several cameras are in farming paddocks) or visibility/awareness depending on what is necessary. **Right:** Billa Kalina DFN camera installation from the reverse angle, which shows the battery and power converter underneath the solar panel and the DFN observation housing on the stand. [Photos courtesy of the DFN wiki, taken by Martin Cupak]

2.1 THE HARDWARE AND DATA STRUCTURE

The development of a camera network in Australia faces unique challenges, with cameras located in regions that are extremely remote, and subject to extreme weather conditions. As a result, the design of the network has been shaped by the nature of the Australian environment. Most of the space in the center of Australia is unpopulated, which makes it perfect for setting up cameras to watch the night sky uninterrupted by light pollution. The first issue encountered with this large expanse of space is the isolation, and therefore the observatories must operate with as little oversight as possible, in other words, they must be autonomous. This autonomy was achieved after several iterations, along with ensuring the cameras are robust enough to survive in the harsh Australian outback. The current iteration of the camera can be seen in Figure 2.1, with a rooftop installation example also seen in Figure 2.2 right. A complete overview of this process can be seen in Howie, Paxman, Bland, Towner, Cupak, Sansom and Devillepoix (2017), which describes the system currently in use and how it evolved to overcome the specific design requirements.

In the left panel of Figure 2.2, the interior of a typical GFO installation can be seen and

noted that the entire housing is quite compact. Inside, there is a Nikon D810 DSLR camera with a Samyang 8mm 3.5F fish-eye CS II lens. The lens has been modified to include a specifically designed liquid crystal (LC) shutter which is modulated with a de Bruijn sequence to encode the fireball timing into the image (see Section 2.1.1 for a more in-depth explanation). This is accompanied by a Watec WAT-902H2 CCIR ULTIMATE video camera (or equivalent), which records minute-long snippets of video to complement the still images and generate light curve information for observed fireballs (Devillepoix et al., 2018).

The camera takes a 25 second long exposure image every 30 seconds, this image is then subjected to the analysis described in section 2.1.1. Every 15 minutes one of these images is analysed further to ensure hard drive space is not being wasted due to inclement weather. This step counts the visible stars in the frame and compares them to the expected number. If these are found to not meet the specified threshold, imaging is stopped and the ability to resume observations is reassessed 15 minutes later (Howie, Paxman, Bland, Towner, Cupak, Sansom and Devillepoix, 2017).

2.1.1 *THE AUTOMATIC DETECTION OF FIREBALLS*

At its simplest, a digital camera consists of a lens and a detector. The lens collects light from the field of view (FOV) and focuses it onto the detector, which results in an image. DSLR cameras are slightly more complex as they can have interchangeable lenses, which allows for different FOVs for different situations. Whilst lenses themselves possess circular apertures, the detector, where the image is projected inside the camera, is rectangular. This results in rectangular images, with the central region of the overall FOV being sampled. For the DFN cameras, a lens with a wide FOV (a fish eye lens) is used, which allows the camera to capture almost the entire sky in every image. A circular image is produced (as seen in Figure 2.3) and displayed on the rectangular sensor with minimal cropping (only at the top and bottom). Typically, the cameras will be

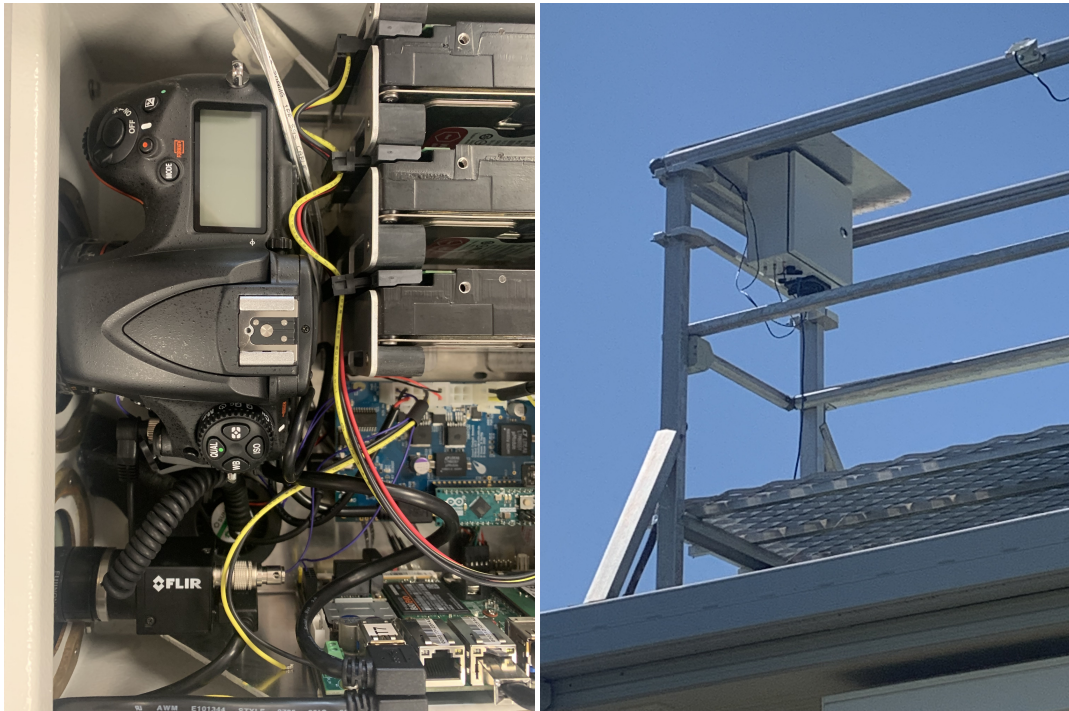


Figure 2.2: These images are of a typical Global Fireball Observatory (GFO) rooftop installation. **Left:** Camera housing internals. From top right in a clockwise direction, you can see the camera, hard drive storage, PCBs, and video camera. **Right:** Housing installation at Mt. Kent observatory, currently awaiting network connection to start operations and collect data. [Photographs taken by the author.]

oriented such that the areas lost are due north and due south, meaning the long axis of the detector is oriented in an east-west direction.

Once the initial image is acquired, the automated analysis begins. First, the image is split into tiles, which are examined for differences between the current and the previous image. A difference is deemed to exist if the values of many pixels in the tile have changed by an amount greater than a certain threshold limit. The tile is discarded from the rest of the process if this limit is not met, along with tiles that are overly saturated, such as those containing the Moon, an example of this can be seen in Figure 2.4. To ensure minimal false positives in this process, a Gaussian blur is applied to images with differences, and the process is then repeated. This process smooths the differences over multiple pixels, essentially blurring the original images to aid in the removal of false



Figure 2.3: **Left:** DN151203.01 fireball observation from the Etadunna observatory on 3 December 2015. Here the de Bruijn sequence encoding is clearly visible within the image as dashes. **Right:** DN151212.03 fireball observation from 12 December 2015, again from the Etadunna observatory. This is the entire frame using a fish-eye lens from a large fireball event. The de Bruijn encoding is not as obvious as the adjacent image, this is because sensors have been saturated by the brightness of the event. This means there is too much light observed in that pixel, and it begins to bleed into the adjacent pixels causing smears.

positives caused by fast-moving stars close to the celestial equator.

The tiles that remain must then be analysed for the fireball streak. This is done using a Hough transform, which checks for straight lines within the image (Duda and Hart, 1972). Figure 2.3 clearly shows the meteor trail as a curve, which is primarily due to the shape of the fish-eye lens. Locally, however, the dashes of the meteor trail are seen as straight lines. The Hough transform works by scanning each image, pixel by pixel to see if lines are formed with other nearby pixels. These lines are found in the Hough space, which uses a different set of co-ordinates from the conventional $x y$ co-ordinate space. This allows for an alternative representation of the same points. Each point in the $x y$ space corresponds to a line in the Hough space which represents the gradient and y -intercept of every possible straight line that passes through that point in the $x y$ space. If you transform multiple points from the $x y$ space to the Hough space, the intersection of these lines in the Hough space represents the straight line that passes through these points in the $x y$ space. Figure 2.5 shows this concept in a visual manner.



Figure 2.4: This figure shows an example of an image that suffers from meteorological interference. Luckily the meteor observed was in a tile far enough away from the Moon that it was still able to be analysed. The image was taken from the Mundrabilla observatory in Western Australia, on the 19th of December 2015.

It is important to be able to find lines in the image, as the fireball will appear as a series of dashes (small straight lines), due to the liquid crystal shutter that encodes the timing of the fireball within the stationary image. The shutter flickers in a set pattern throughout the exposure time, which allows timing and velocity data to be determined from each image (Howie, Paxman, Bland, Towner, Cupak, Sansom and Devillepoix, 2017). The flickering of the shutter cuts the fireball trail into a series of dashes. This particular pattern of dashes is known as a de Bruijn sequence. The sequence was chosen to encode the fireball timing information directly into the image, thereby removing the need for a secondary system for absolute timing (Howie, Paxman, Bland, Towner, Sansom and Devillepoix, 2017). The de Bruijn sequence is the shortest possible cyclic sequence to include all permutations of a subsequence of a specified length for a given

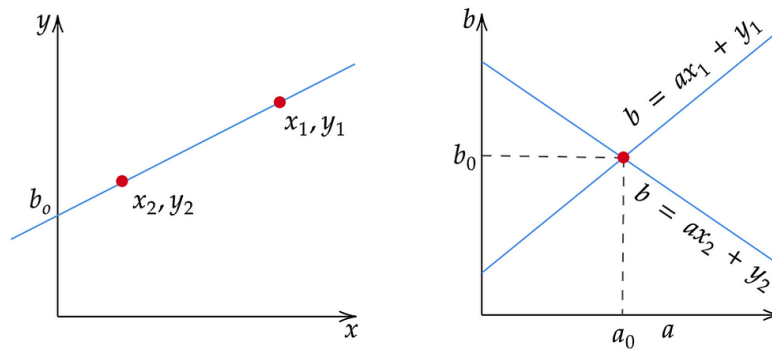


Figure 2.5: Here the plot on the left shows the two points in the $x y$ space, while the plot on the right shows these points represented in the Hough space. The intersection of these lines in the Hough space (in the right-hand graph) corresponds to the line that passes through both of these points in the $x y$ space (the left-hand graph). Image borrowed from Lee (2020).

alphabet (Flye Sainte-Marie, 1894; de Bruijn, 1946). For example, if our alphabet has two elements $\{a, b\}$, and our subsequence length is three, one of the possible de Bruijn sequences would be, “aaabbbab”. This sequence contains the eight possible subsequences of length three (aaa, aab, abb, bbb, bba, bab, aba, baa). As the sequence has a cyclic nature the last two sequences can be made by taking elements from both the end and the start of the whole sequence (see Equation 2.1 below for a visualisation).

$$\begin{array}{cccccccc}
 [a & a & a] & b & b & b & a & b \\
 a & [a & a & b] & b & b & a & b \\
 a & a & [a & b & b] & b & a & b \\
 a & a & a & [b & b & b] & a & b \\
 a & a & a & b & [b & b & a] & b \\
 a & a & a & b & b & [b & a & b] \\
 \dots a] & a & a & b & b & b & [a & b \dots \\
 \dots a & a] & a & b & b & b & a & [b \dots
 \end{array} \tag{2.1}$$

A probabilistic Hough transform (Duda and Hart, 1972) is then employed to identify these line segments as part of a larger line that stretches across the image. This type of

Hough transform is used to cut down on computational needs, as it is less resource intensive. This method does require a binary image which can be achieved by running the image through the Otsu algorithm (Otsu, 1979). The Otsu algorithm classifies the image into a binary image, by classifying each pixel as either being in the foreground or the background. Astronomical images are ideally suited to this type of analysis as they are bright light sources with dark backgrounds, giving a clear distinction between these two sets of data.

Finally, to minimise false positives a series of physical parameters are checked. The brightness of pixels is analysed to ensure the variations are consistent and peaking toward the center, along the length of the line. If it is found that the line peaks toward the ends, it is likely to mean multiple stars in close proximity are the cause. The coordinates of the line are checked, which will remove slow-moving or stationary objects that have been ‘mistaken’ for lines by the Hough transform. In reality, they are multiple stars close together in the case of stationary points or objects like satellites or planes for slow-moving ones. If too many lines, over 10,000, are found in the tile being analysed it can be discarded, due to these lines being the edges of clouds.

2.1.2 COLOUR EXTRACTION

The DFN uses an off-the-shelf camera and lens system in their observatories. Section 2.1 explains that the fish-eye lens has been modified with an LC shutter which has been specifically designed to encode timing into the image. The total exposure time of each image is 25 seconds, this is called the duty cycle, and it is broken up into both open and closed portions of the LC shutter. The duty cycle fraction,

$$D_c^o = \frac{T_0^o}{T_0}, \quad (2.2)$$

is used in the flux calculations. In this equation, T_0^o is the time that the LC shutter is open, and T_0 is the total exposure time of each image. Note that when the LC shutter is closed it is not perfect, which means that there is a small portion of light transmitted through the shutter when closed. However, in practice, this can be thought of as zero. In theory, this is known as the transmittance ratio and is represented by

$$E = \frac{f_0^c}{f_0^o}, \quad (2.3)$$

where f_0^c is the flux on the sensor when the LC shutter is closed, and f_0^o is the flux when the LC shutter is open. I_0 , the electron count, can be used to find the total flux when the LC shutter is open (f_0^o), and this can be calculated using:

$$f_0^o = \frac{I_0}{T_0(D_C^o + E(1 - D_C^o))}, \quad (2.4)$$

which reduces to,

$$f_0^o = \frac{I_0}{T_0(D_C^o)}. \quad (2.5)$$

From this, the apparent magnitude of the objects using the instrument (m_0^{inst}) can be found and used for, firstly calibration of the observatories, and secondly the magnitude of the fireballs themselves. The instrument magnitude can be found using,

$$m_0^{inst} = m_0 + 2.5 \log(f_0^o) + kX_0, \quad (2.6)$$

where m_0 is the apparent magnitude of a catalog star, k is an extinction coefficient that depends on the colour channel (R, G, or B), and X_0 is the airmass between the meteor and the observatory. This equation describes the apparent magnitude of a chosen star through the observatory and can be used to calibrate the observatory to find the apparent and absolute magnitude of a fireball. Using this calibration equation, the apparent magnitude of the meteor can be found with:

$$m_f = m_0^{inst} - 2.5 \log(f_f) - kX_f, \quad (2.7)$$

where X_f and k are the same as in the previous equation, and f_f is the amount of flux for a de Bruijn sequence dash, defined by

$$f_f = \frac{I_f}{T_f}. \quad (2.8)$$

Here I_f is the electron count normalised by the exposure time, and T_f is the length of the box that encapsulates the de Bruijn sequence dash. A further and more in-depth explanation of this as well as accompanying images can be found in Devillepoix (2018).

The Bayer colour filter construction (Bayer, 1976) leads to the fact that there are two times as many green sensors as red or blue ones. This means that naturally, the camera is more sensitive in the green colour channel, whereas the red and blue channels suffer from low signal to noise in some cases. The green colour channel is sufficient to perform the trajectory and orbital calculations used in the DFN database. However, this does mean that colour-indices can not be calculated for the affected observations.

As mentioned in Section 1.5, the colour-indices can be used to create a velocity relation, which if successful could allow for meteor shower association to be suggested or confirmed from single camera observations. Jacchia (1957) and Hajdukova (1974) used photographic and naked eye observations to construct the colour-index used in their study, which is most comparable to a B–V colour-index with more modern equipment. Given that the Bayer colour filter is constructed to closely mimic the human eye, the colour-index most analogous to the data in this study is B–G. B–R and G–R are also computed, but present a different relationship and are not able to be compared to any previous results found in the literature.

2.1.3 FIREBALL TRAJECTORY DETERMINATION

If a fireball is identified from one of the images, there are a few reliable methods to predict where meteorites may be found if one were to survive the ablation process and impact the ground. Ceplecha (1987) proposed one of the first methods of determining fireball trajectories using the method of planes, which involved using line-of-sight measurements and the position of at least two observing stations. Borovicka (1990) offered a different method with the straight-line least-squares (SLLS) method, which resulted in smaller residuals if the initial measurements were of high enough quality for the use of the method.

The SLLS method essentially works the same as linear or multiple regression, it finds the best fit flight path of the meteor. It uses the observations from all cameras and finds the trajectory that best suits the data. This differs from the method of planes, where the observatory and the start and end point of the fireball construct a plane and the trajectory is found to be the intersection of these planes. These methods use trigonometric and geometrical means to estimate the flight path of the fireball and then are extrapolated in either direction and used in conjunction with other key parameters to gain insights into the possible fall location or orbital path. Figure 2.6 gives a basic visual representation of the two methods, with the SLLS method of the left and the method of planes on the right.

As the quality of the observations and the equipment used to record them has increased, it has become possible to use more complex statistical methods in order to analyse these events with increasing accuracy. While the SLLS method is still widely used (Devillepoix et al., 2018), other methods such as the particle filter (Sansom et al., 2017) and the extended Kalman filter (Sansom et al., 2015) are being used to great effect. These three methods are used in conjunction to better map dark flight, give orbital information, and provide tighter constraints on possible search areas.

Comparison of Straight Line Least Squares and Method of Planes

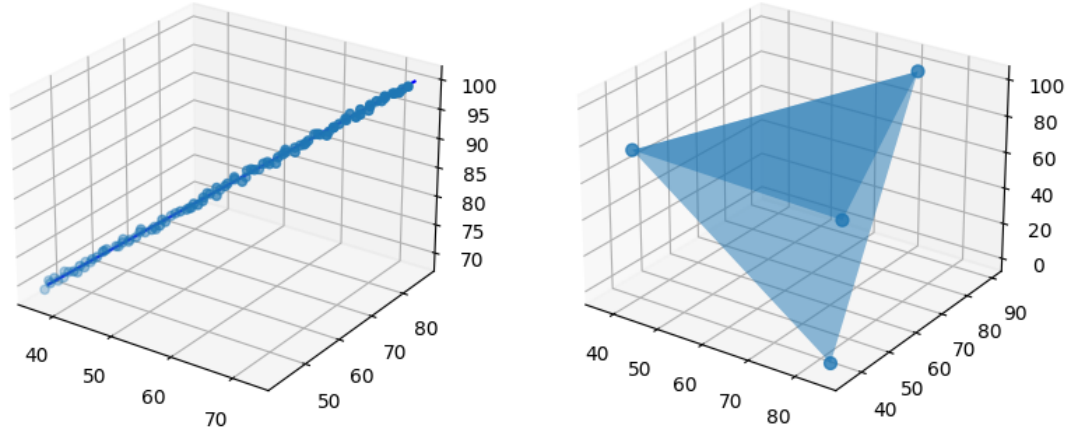


Figure 2.6: Left: This is a visual representation of the SLLS method. The line of best fit can be seen to pass through the middle of the points and would give the trajectory of the meteor in its bright flight phase. **Right:** Shows how the method of planes is used to construct the trajectory of the meteor in its bright flight phase. A plane is drawn between the observing station and the start and end points of the meteors bright flight phase. This is done from all stations that observe the given meteor and the trajectory is calculated to be the intersection of the planes.

These extrapolations of fall locations or orbital paths are important for different reasons. Accurate fall locations allow for tighter constraints on possible search areas. This is increasingly important given the distances and terrain needed to be traversed in Australia in efforts to recover meteorites. To help combat this, and minimise search time, camera drones have been tested and used in conjunction with machine learning algorithms. These tests have already achieved promising results to aid in the search for meteorites (Anderson et al., 2019; Citron et al., 2021), with the recent recovery of the first meteorite using this method (Anderson et al., 2022). Knowing the orbital trajectories of meteors helps in defining the population estimations and their origins (Nakamura et al., 2011). This information could be used in the future to help assess possible targets for asteroid mining or likely origins of future large Earth impactors (Vernazza et al., 2008).

3

PAPER 1 - COLOUR ANALYSIS OF METEORS USING THE DESERT FIREBALL NETWORK

3.1 SUBMITTED PAPER

This is the first paper in my Masters project, Todd et al. (2023). This work presents a pilot study using RGB colour of fireballs, which will later be used on the complete Desert Fireball (DFN) dataset. This paper was submitted on February 28, 2023 to The Monthly Notices of the Royal Astronomical Society. This paper was submitted under my publishing name Christopher J. Todd., which I have chosen to be more unique than my surname (Johnson) and I will be continuing to publish under this name for future works.

Before the submission of this work, I received feedback from the reviewer, resulting in changes to the paper and consequently my thesis. These have been implemented in the paper and throughout the thesis. The paper is currently being vetted by my co-authors and will be re-submitted on or before the 14th of April 2023.

3.2 ABSTRACT

In this work, we present an analysis of the colours of fireballs observed by the Desert Fireball Network (DFN) in November and December 2015. We determine a set of colour-indices for each observed fireball in the dataset and use the resulting data to perform a comparative study between the different meteor showers and sporadic meteors represented in the data. From the data presented in this preliminary study, we find a relationship between the initial velocity of an incoming fireball and the colour-index at an altitude of 75 km, which matches previous literature values. Previous studies have suggested that meteors become bluer at slower velocities. In this work, we see signs of a similar trend, though the statistical significance of the result is limited due to our low sample size. The study also found a disconnect between the closely related Northern and Southern Taurids which will need further investigation to explain completely. The result of this pilot study can be used to better define a velocity, colour-index relation which could be used to classify fireballs into showers from single camera observations where trajectory and orbit data can not be calculated.

Colour Analysis of Fireballs from Late 2015

Christopher J. Todd,^{1*} E. K. Sansom,^{2,3} H. A. R. Devillepoix,^{2,3} J. Horner,¹ M. C. Towner,² M. Cupak,^{2,3} D. Wright,¹ B. Carter¹

¹*Centre for Astrophysics, University of Southern Queensland, Toowoomba, Queensland 4350, Australia*

²*Space Science and Technology Centre, School of Earth and Planetary Sciences, Curtin University, GPO Box U1987, Perth WA 6845, Australia*

³*International Centre for Radio Astronomy Research, Curtin University, Bentley, WA 6102, Australia*

Accepted XXX. Received YYY; in original form ZZZ

ABSTRACT

In this work, we present an analysis of the colours of fireballs observed by the Desert Fireball Network (DFN) in November and December 2015. We determine a set of colour-indices for each observed fireball in the dataset and use the resulting data to perform a comparative study between the different meteor showers and sporadic meteors represented in the data. From the data presented in this preliminary study, we find a relationship between the initial velocity of an incoming fireball and the colour-index at an altitude of 75 km, which matches previous literature values. Previous studies have suggested that meteors become bluer at slower velocities. In this work, we see signs of a similar trend, though the statistical significance of the result is limited due to our low sample size. The study also found a disconnect between the closely related Northern and Southern Taurids which will need further investigation to explain completely. The result of this pilot study can be used to better define a velocity, colour-index relation which could be used to classify fireballs into showers from single camera observations where trajectory and orbit data can not be calculated.

Key words: meteorites, meteors, meteoroids – comets: general – planets and satellites: general – catalogues – methods: observational – techniques: photometric

1 INTRODUCTION

Our Solar system contains a vast amount of debris, left behind from the formation of the system. That debris spans a vast range of sizes, from innumerable small dust grains to asteroids, cometary nuclei, and even dwarf planets¹. The smallest pieces of debris are by far the most common, and are widely referred to collectively as ‘meteoroids’. These range in size from microscopic dust grains (also known as Brownlee particles, e.g. Ganapathy & Brownlee 1979) up to objects one metre in diameter (with larger objects considered to be either asteroids or comets; e.g. Rubin & Grossman 2010). The Earth is bombarded with between five and 250 metric tons of cosmic debris per day (Love & Brownlee 1993; Bland & Artemieva 2006; Plane 2012), where the largest can be observed to produce meteors, fireballs (meteors brighter than an apparent magnitude of -4), and bolides (fireballs that explode during flight; e.g. Campbell-Brown et al. 2013).

Meteoroids are produced through a number of different mechanisms. Some are created as a result of collisions between objects in the asteroid belt, whilst others are shed by cometary activity (e.g. Carlson et al. 2003). As the Earth moves through its orbit, it often crosses trails of debris laid down by asteroids and comets. These

debris streams cause the many meteor showers that occur through the course of the year (see Ceplecha et al. 1998; Jenniskens 2006). As the debris that causes a given meteor shower are roughly on the same orbit as one another, the resulting meteors appear to radiate outwards from the same patch of the sky, known as the radiant. If a meteor is observed that can not be associated with any known shower, it is designated as a ‘sporadic’ (Ceplecha et al. 1998).

Modelling has suggested that between ~80-95% of sporadic meteors have a cometary origin, with the majority having been produced by Jupiter family comets and then having sufficiently dispersed such that any connection between a specific meteoroid and particular comet can no longer be made (e.g. Nesvorný et al. 2010; Soja et al. 2019, among others). This indicates that the majority of both sporadic and shower meteors are composed of cometary material. However, when one considers the largest objects to impact the Earth’s atmosphere, this is not the case. For fireballs bright enough to potentially drop meteorites, it is established that the great majority are asteroidal in origin (Shober et al. 2021). This ties in with our current knowledge of the impact threat posed by even larger objects – with most sources in agreement that the majority of the impact threat to the Earth comes from the Near-Earth Asteroid population, rather than the short- and long-period comets (DeMeo & Binzel 2008; Belton et al. 2011; Mainzer et al. 2011).

As a result, the majority of particles bombarding our planet daily will go essentially unnoticed, being made up of dust particles smaller than 100 μ m (Ocaña 2017). Meteoroids of at least mm to

* E-mail: u1141791@usq.edu.au

¹ A detailed description of the Solar system as a whole is beyond the scope of this work - but we direct the interested reader to Horner et al. (2020) and references therein.

cm-sized scale are required to produce fireball events, and it is these events that we study in this work. As such, our data likely straddle the turning point at which asteroidal material begins to dominate over that of a cometary origin - with the brightest fireballs being almost exclusively sporadic events of asteroidal origin.

The meteoroids we observe will still include objects with both asteroidal and cometary origins. The majority of meteor streams are thought to have cometary origins,². As such are very unlikely to drop a meteorite, due to the friable nature of cometary material. Sporadic meteors do not possess known shower associations, which gives the potential they are of asteroidal origin and therefore more likely to drop a meteorite (e.g. Devillepoix et al. 2018; Jenniskens et al. 2019; Sansom et al. 2020; Anderson et al. 2022), if a large enough meteoroid enters the atmosphere.

An existing method by which the cometary or asteroidal origin of a given object can be estimated is through the calculation of the Tisserand parameter of the object's orbit, with respect to Jupiter (T_J). In simple terms, a value for T_J greater than three typically indicates that the orbit of the object in question moves either exclusively interior to or exterior to that of Jupiter (Radau 1896; Murray & Dermott 2000). This distinction has, in the past, proven a useful general method by which cometary and asteroidal objects can be distinguished on the basis of their orbital elements alone, and has even been the basis of proposed classification systems for Solar system small bodies (e.g. Kresák 1972; Levison & Duncan 1994; Horner et al. 2003).

Exceptions to the rule do occur³, and it should be noted that T_J is only approximately conserved during encounters with Jupiter - so if a small body's orbit is perturbed by another planet, or experiences orbital modification through non-gravitational forces, that would cause T_J to change (numerous examples of which can be seen in e.g. Horner et al. (2004a,b)). As such, T_J primarily serves as a useful tool by which one can obtain a first estimate of the nature of a given object, but is not sufficient in and of itself to constrain the origin and history of a given Solar system body. Indeed, Shober et al. (2021) found that a significant fraction of meteors observed using the DFN that were clearly members of known meteor showers with cometary parents moved on orbits with $T_J > 3$, which would normally suggest an asteroidal origin for that debris. As such, it seems particularly challenging to use the value of T_J alone to constrain the origin of meteoric material observed with the DFN, although the Tisserand parameter nonetheless remains a useful tool for grouping objects that display similar orbital/dynamical behaviour.

Asteroids and comets, the parents of these meteor streams, are themselves the remnants of the planet formation process. They are key to studying how our planetary system formed and evolved to its current state. The ability to study samples of

those objects in the lab is therefore extremely valuable, allowing us to gain far more information on their history than can be obtained from distant observations alone (see e.g. Ceplecha et al. 1998; Carlson et al. 2003; Horner et al. 2020, and references therein).

Sampling asteroids directly is, however, an expensive endeavour, relying on sample return missions (e.g. JAXA's Hayabusa and Hayabusa2 missions, and NASA's OSIRIS-REx; Yoshikawa et al. 2021; Sugita et al. 2020; Dworkin & Osiris-Rex Team 2017). The best information we can gather for the vast majority of asteroids and comets comes from observations of their reflectance spectra, whose features and shapes are determined by their surface geochemistry (e.g. Tholen 1984; Bus 1999; DeMeo et al. 2009).

Meteorites offer a direct solution to this problem. If we are able to link meteorites to their parent bodies, we can gain significant insights into the geochemistry of distant asteroids. However, even with a reliable orbit, the chaotic nature of the solar system makes it difficult to unambiguously link a sample to a unique parent body. Of the ~70,000 meteorites that are currently held in collections around the Earth, pre-atmospheric orbits are only available for ~50 (e.g. Grossman 2005; Meier 2017). Beyond a physical sample, we may study the spectra of meteors as they transit through the atmosphere. Historically, this too has proven challenging, since high resolution spectrometers usually have very narrow fields of view. This results in the capture of meteor spectra being highly serendipitous events. Borovička et al. (2005) classified 97 meteors using their spectra, with 64% having pre-atmospheric orbits available to discuss parent body origins. Sporadic meteor spectra are rarer and less predictable than the members of the major meteor showers, especially those that would lead to fireball and meteorite-dropping events. In order to obtain a large sample of such events, it is necessary to deploy detectors on a continental or planetary scale, to maximise the amount of the Earth's atmosphere being observed at any given time, and therefore increase the odds of such events being observed and recorded.

Whilst measurements of the spectra of meteors and fireballs are particularly valuable, it is currently not feasible to deploy high-resolution spectroscopic equipment on all-sky cameras distributed on a continental scale. Fortunately, an alternative to high-resolution spectrometry is to simply look at the Red/Green/Blue colour of a meteor in an optical image (photometry). In essence, such photometric observations yield a quasi low-resolution spectrum of the observed event. These kinds of observations require much simpler equipment and serve as a cheaper and easier method of observing these phenomena. Although such observations lack the precision of spectrometry, this disadvantage can be partly overcome by the vastly larger amounts of data that can be observed, collected and reduced. Photometry of RGB images extracts a value for each colour channel (in this case, one for each of the red (R), green (G), and blue (B) sensors) in the Bayer colour filter of a DSLR camera. The resulting RGB colour can be used to help the simple classification system already in place, thanks to studies done with spectra. Investigating whether colour variations in RGB observations produce noticeable differences or consistent trends, for meteors in a given shower, could enable:

- (i) more efficient differentiation between sporadic meteors and members of known showers,
- (ii) the identification of meteors that share a common origin to members of known showers, but that now move on orbits markedly

² Examples include the Quadrantids (parent comet likely 96P/Machholz; e.g. McIntosh 1990; Jenniskens 2004; Ye & Jenniskens 2022), the Leonids (parent comet 55P/Tempel-Tuttle; e.g. Yeomans 1981; Yeomans et al. 1996; Asher et al. 1999), and the Perseids (parent comet 109P/Swift-Tuttle; e.g. Marsden 1973; Wu & Williams 1993; Williams & Wu 1994)

³ Such as comet 2P/Encke, which is dynamically decoupled from Jupiter, and hence has T_J greater than three; the Jovian Trojans (many of which have T_J less than three), and icy bodies like comet 29P/Schwassmann-Wachmann and the Centaurs, which orbit entirely in trans-Jovian space and thus again have T_J greater than three.

different to their siblings (that would otherwise be identified as ‘sporadic’ meteors). Or, new meteor showers from meteors that have been categorised as sporadic due to their low observation rate,

(iii) tighter constraints on a meteor’s physical parameters, allowing for shower associations to be considered or potentially confirmed from single camera observations, though the use of a velocity relation.

The use of colour to categorise meteors has been touched on previously, most notably by Moorhead & Kingery (2020). Using data from Vojáček et al. (2015) and the classification system laid out by Borovička et al. (2005), Moorhead & Kingery (2020) were able to simulate meteors seen by RGB colour filters to show that iron-type meteors were both bluer and less red than others in the same dataset (higher B-R colour-index). Due to the small nature of the dataset in question, no further conclusions were able to be drawn. However, this demonstrates the potential of using RGB colour to categorise meteors into a taxonomy.

Hajdukova (1974) went one step further, and investigated the dependence of meteor colour on a variety of factors. At the time, only black and white photographs were available, but the authors built upon work by Jacchia (1957), in which the colour-index was based on the combination of naked-eye and photographic observations of individual meteors. Since the photographic film used was markedly more blue-sensitive than the human eye, they obtained a colour index by calculating the photographic and naked-eye magnitudes, subtracting one from the other – giving a value that is broadly analogous to modern B-V measurements. Hajdukova (1974) concluded that the colour-index of a meteor ‘increases’ with increasing velocity at a rate of between 12 and 16 mmag per km/s⁴. In other words, they found that slower meteors were bluer than their faster counterparts. In this work, we make use of colour-indices calculated from modern RGB images, noting that the colour-index developed by Hajdukova (1974) is most directly comparable to the calculations of B-G colour-index used in this study.

The specific use of RGB colour as a means to categorise meteors or fireballs has not been attempted on large scales as there has not previously been enough RGB data. The Desert Fireball Network has more than 50 cameras across Australia and has expanded to form the Global Fireball Observatory (GFO) with ~100 cameras across seven countries, spanning six continents (Devillepoix et al. 2020). The GFO are one of few camera networks to observe in colour, putting them in the unique position of having large data volumes from the planet-scale detector for these objects. As such, in this work, we describe the results of a pilot study using observations of fireballs from November and December of 2015, in which we analyse the RGB colour-indices of DFN fireballs over Australia (southern hemisphere). This data encompasses fireballs from the Taurid and the Geminid meteor showers, along with many minor showers and sporadic events (full list in Table 1). We compare fireball colour indices and the physical parameters calculated for each event (see e.g. Sansom et al. 2015, 2017; Howie et al. 2017; Towner et al. 2020, for more details).

⁴ It’s worth noting that ‘increasing’ in this case actually refers to a fainter meteor, due to the inverse nature of magnitude measurements.

2 DFN DATA COLLECTION

The Desert Fireball Network (DFN) is a series of automated observatories specifically designed to detect and make precise observations of fireballs from multiple locations, in order to triangulate the potential region in which any resulting meteorite might fall. To date, more than fifty of these stations have been deployed across several states in Australia, the majority of which are in the Western and South Australian outback (Devillepoix et al. 2020). This provides a large coverage of the night sky for maximal opportunities to observe fireball trajectories. The Australian outback is uniquely suited for fireball observation and meteorite recovery, with vast areas void of population and therefore light pollution, and barren mono-tonal terrain for optimal meteorite search and recovery.

Each DFN observatory is equipped with an RGB (red, green, and blue) DSLR (Digital Single Lens Reflex) camera with a fish-eye lens (see Howie et al. 2017, for details), which takes long-exposure images of the sky all night, every night, whenever the observatory has clear skies (e.g. Figure 1). When a fireball is observed in this manner, it is automatically detected by specifically designed software (described in Towner et al. 2020). The data obtained by every camera that sighted the fireball is then reduced (as described in Devillepoix et al. 2018). This allows the DFN to constrain the orbital origins of a meteoroid, with physical and entry parameters computed in alignment with Sansom et al. (2017, 2019) and Jansen-Sturgeon et al. (2019).

Each DFN camera continuously takes 25 second exposure all-sky images every 30 seconds in RGB. Each image is encoded by a liquid crystal (LC) shutter, which allows precise timing and velocity information to be extracted from each image. To extract the data we must consider three main things:

- (i) The camera is equipped with a Bayer array which has twice the number of green sensors as individual red or blue sensors. This means that a different scaling factor must be applied to the data from the red and blue sensors to gain the true apparent magnitude of the fireball from the image in those colours.
- (ii) The total exposure of the frame is 25 seconds, however, this is offset by the LC shutter. Correction factors must be added for these effects.
- (iii) The fish-eye lens distorts the image as it takes in a whole sky view. This means that more of the sky is concentrated on less of the sensor pixels as you move toward the outer edges of the image. This also means that light from stars and other bright objects needs to travel through more atmosphere toward the edge of the image and therefore more light is scattered and they appear less bright.

A more in-depth discussion of these points can be found in Devillepoix (2018). To gain magnitude measurements from an image, firstly, calibration is performed using background stars to obtain an instrument magnitude (apparent magnitude of a known background star when viewed through the instrument). This measurement is different for each colour band. The instrument magnitude, along with the correction factors (for each colour band), can then be used to sum the incoming flux from a fireball (for each dash in the de Bruijn sequence⁵, and calculate the apparent magnitude of the fireball at each point along its bright flight trajectory Devillepoix (2018).

Due to the nature of the Bayer array, not all channels (RGB)

⁵ A visual example of the de Bruijn sequence can be seen in Figure 1.

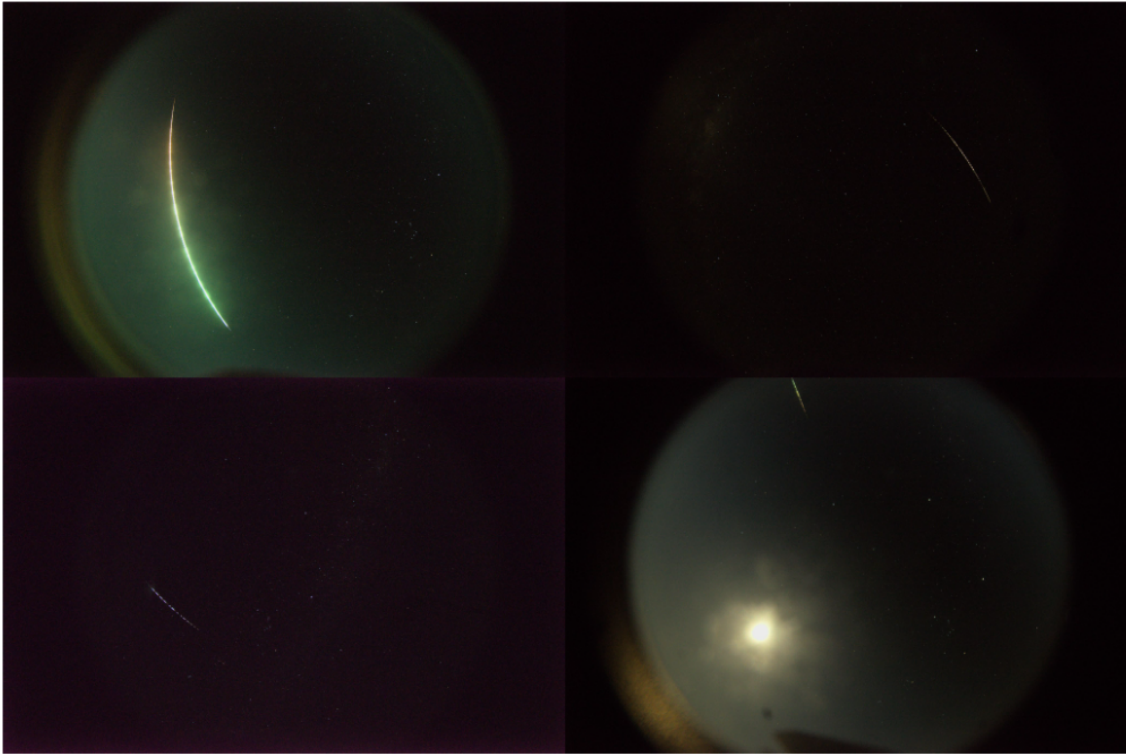


Figure 1. This figure shows four examples of fireball colour images, taken from the Etadunna (DN151212–03), Barton (DN151105–01, data also in Figure 2), Mundrabilla (DN151219–01), and Ingomar (DN151217–01) observatories in a clockwise direction from the top left. The Etadunna observation in the top left was the longest duration fireball in the study at just under 13 seconds. The top right and bottom left panels show typical fireballs observed, with the bottom left appearing bluer. The bottom right image gives an example of why the method described in [Towner et al. \(2020\)](#) is necessary to eliminate unwanted objects in the image.

can be extracted from each image due to having low signal-to-noise. This results in some images only having data in the green channel, which is enough to perform trajectory analysis but will exclude them from this colour investigation study. Due to the long exposure, the saturation of certain pixels can become an issue within the images. This usually happens with a full Moon (seen in the bottom right panel of Figure 1) or other ground-based anomalies (street and car headlights). Such images are processed and handled accordingly with the onboard computing packages ([Towner et al. 2020](#)). However, this does become an issue with some of the brighter fireballs as the camera has a limiting magnitude of about $m_V = -8$. The impact of this limiting magnitude can be seen in the top left panel of Figure 1, where the sequences of dashes appear to overlap and bleed into adjacent pixels.

3 DATASET AND ANALYSIS

The Desert Fireball Network (DFN) possesses large amounts of archival data on fireball observations from various locations around Australia. For this study, data from November and December of 2015 has been used, which includes data from several major showers (Northern and Southern Taurids, and Geminids), many members of minor showers (see Table 1), as well as many sporadic observations

(see Table 1 for a full list of showers represented in the dataset, and the number of fireballs observed for each). Of the 229 events in the study period, 68 of the events had to be discarded due to either being too faint, or obscured by meteorological interference of bright moonlight (the effect of the Moon can be seen in the bottom right panel of Figure 1). After these events were removed, we were left with a sample of 161 unique events (383 observations) for which the data was of high enough quality to allow more detailed analysis.

An example of a fireball event that was observed from multiple DFN locations can be seen in Figure 2. This figure shows, in the left panel, the *apparent* magnitude data from five observations from the Mulgathing, Ingomar, Barton, Mount Barry, and William Creek observatories (The raw image from the Barton observatory can be seen in the top right panel of Figure 1). Saturated data points can be seen as crosses of the same colour as the filter in which they were recorded. Four of the five observations yield data from all three colour channels (RGB), with the observation from the Barton DFN camera only providing usable data from the green channel. Note that due to the differences in range and seeing conditions, the apparent magnitudes vary between cameras, but the trend is consistent overall. Figure 2 shows the same data as a series of colour-indices against time. It can be seen that, although the observed apparent magnitude of the fireball varied significantly between observations

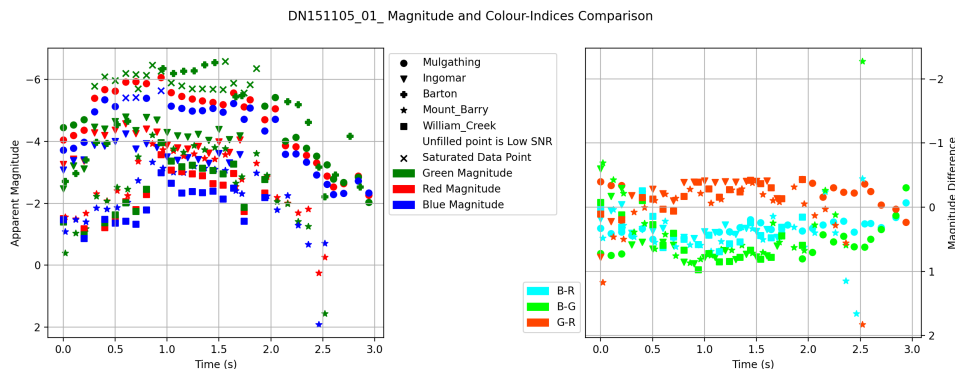


Figure 2. This figure shows an example of the processed apparent magnitude and colour-index data for one fireball event, from the 5th of November 2015, possessing multiple observations from different DFN stations (top right panel of Fig 1). In the left panel, we find the apparent magnitude of the RGB colour channels for each station; Mulgathing, Ingomar, Barton, Mount Barry, and William Creek. The saturated data point can be seen as crosses and encompasses data from the Barton and Mulgathing stations. In the right panel, the available colour-indices can be seen. No colour-index data from the Barton observation can be seen as there was only data from the green filter available. It can also be noted that the G-R and the B-G results are sparse throughout the centre of the observation time as the Mulgathing green filter became saturated.

from different cameras (due to factors including the weather, and the distance from the camera to the fireball), and over time from any given station, the colour-indices remain relatively constant between observatories and through the flight of the fireball.

When calculating the average colour-index for each colour channel we remove the first and last 10 percent of the data collected. This is to avoid low signal to noise sections (beginning and end) of the fireball. From the triangulated data, other parameters can be calculated, such as entry radiant and initial velocity. These are used to determine the likelihood of an event being linked to a specific meteor shower (discussion of such parameters and mechanisms are beyond the scope of this work, see [Kasuga & Jewitt 2019](#), for further information). It must be noted, that when analysing color-index values based on apparent or absolute stellar magnitudes, that smaller (more negative) numbers are a stronger signal (brighter). For example, a negative B-R value would be more blue than a positive B-R value. We have added labels to our results plots to help with interpretation.

4 RESULTS AND DISCUSSION

Figure 3 shows the suite of fireball radiants observed, where fireballs are designated members of a shower based on their radiant. Sporadic fireballs in this sample show random scattering. This particular sample of data does introduce a couple of small biases, due to the position of the cameras in the Southern Hemisphere, and the time of year when the observations were recorded (November and December 2015). This puts constraints on the extent of radiants that can be observed (lower-left quadrant of Figure 3). The time of observations introduces a velocity trend with Right Ascension (top left panel of Figure 4). This can be explained by the rotation of the Earth, with incoming fireballs appearing slower in the evening (catching up to Earth) and faster in the morning (head on collisions). The future inclusion of data from all months of the year would help to mitigate these bias for the sporadic dataset, with a given RA and Declination location being found in the morning and evening sky at different times of the year.

Lower initial velocities allow the meteors to penetrate deeper into the atmosphere before ablation begins, and, coupled with entry angle, can lead to a longer bright flight phase (which can be seen to match the trend in the lower right panel of Figure 4). The duration of a fireball, its velocity, and the penetration heights will all influence the colour of the event, regardless of shower/sporadic origin. As velocities are inherently linked to shower origin, colour variations linked to velocity differences may enable shower identification from colours. However, in using colour to infer properties of asteroid parent bodies, determining unique shower characteristics will require decoupling these effects.

Figure 4 and Table 1 show the distribution of physical parameters of the events seen within the observing period of November and December 2015. Figure 4 shows how the initial height and velocity can be clustered by shower ([Whipple & El-Din Hamid 1952](#); [Whipple 1983](#)). The top two panels of Figure 4 show how events from the same stream possess similar initial parameters with constrained ranges compared to the sporadic events, whilst the bottom panels show the bright flight time of each fireball against the initial height of the bright flight phase. The bottom left panel differentiates the meteor showers by colour and marker style, whereas in the bottom right panel, the colour is representative of the initial velocity of the bright flight phase of the fireball. Straight away we can see that there is a correlation between flight time and initial height. But also that shower material rarely begins ablating below 80 km altitude or have flight times longer than 2 seconds. Table 1 summarises the averages and ranges of these physical parameters across showers with multiple observations.

A significant amount of research has been conducted on the origins of meteor showers ([Whipple & El-Din Hamid 1952](#); [Whipple 1983](#)). With common orbital parameters (calculated from triangulated radiant data), each member associated with a particular shower will present with similar fireball parameters, such as initial velocities and subsequently initial ablation heights (such similarities can be seen in Figure 4). Their common bulk material strengths will result in

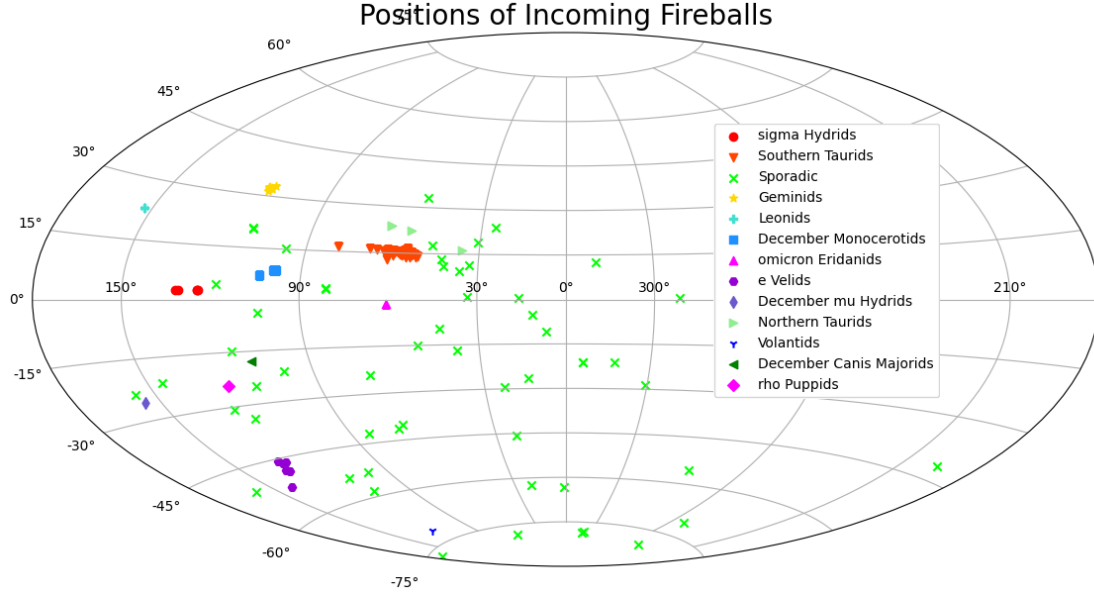


Figure 3. Shows the incoming fireball positions in equatorial co-ordinates, indicating where they started their bright flight phase in the atmosphere. Throughout this paper, this figure can be used as a reference to locate the radiant position of the showers represented in this study. If a shower has more than one observation, it can easily be seen that they cluster together as expected. While sporadic fireballs can be seen scattered across the figure.

Table 1. Summary of the physical parameters observed for sporadic fireballs and each shower group, given as the calculated average and standard deviation to indicate variance in the data for each group (the standard deviation is not given for showers with single observations).

Shower	Events	Initial Values			Flight Time (sec)
		Velocity (m/s)	Angle (deg)	Height (m)	
Sporadic	61	$28,500 \pm 15,800$	47 ± 16	$84,200 \pm 13,500$	1.78 ± 1.66
Southern Taurids	65	$30,400 \pm 1,800$	39 ± 8	$90,300 \pm 4,000$	1.24 ± 0.48
Geminids	8	$35,900 \pm 900$	28 ± 3	$92,200 \pm 3,300$	1.30 ± 0.61
Northern Taurids	7	$28,700 \pm 9,400$	33 ± 7	$88,800 \pm 3,500$	1.87 ± 0.37
e Velids	6	$43,400 \pm 700$	55 ± 13	$89,800 \pm 2,400$	0.60 ± 0.13
sigma Hydrids	5	$60,100 \pm 600$	39 ± 12	$103,200 \pm 2,100$	0.77 ± 0.20
December Monocerotids	3	$43,100 \pm 800$	36 ± 11	$99,200 \pm 2,600$	0.82 ± 0.27
Leonids	1	71,800	22	105,700	0.56
omicron Eridanids	1	28,800	48	79,800	0.57
December mu Hydrids	1	65,400	40	109,500	0.49
Volantids	1	32,500	49	87,300	1.02
December Canis Majorids	1	44,000	56	94,500	0.54
rho Puppids	1	58,600	63	105,000	0.39

similar durability or fragmentation profiles and flight times.

To investigate further, the colour-indices (B-R, B-G, and G-R) are calculated for each of the observed fireballs where each colour band could be extracted above noise levels. The results can be seen in Figure 5 and in Figure 6 where the colour-indices for a fireball at an altitude of 75 km is plotted. Figures 5 and 6, and Table 2 display the average colour-indices for the fireballs with available data. From Table 2, the number of events plotted for each shower can be seen in brackets throughout the table.

When looking into individual shower characteristics, there is a small divergence in the average colour-indices between showers, though only the Northern Taurid fireballs (2 events; right column Figure 5) appear to be more green and less red (overlapping uncertainties). The centre and left panels show that the Sigma Hydrids may be more blue (less red and green) than all other streams (with more than one data point). These results indicate that the Northern Taurid meteor stream may be showing a difference in composition between it and other meteor streams. With the majority of results overlapping within error, a Welch's t-test was used to determine the significance of these results. This test,

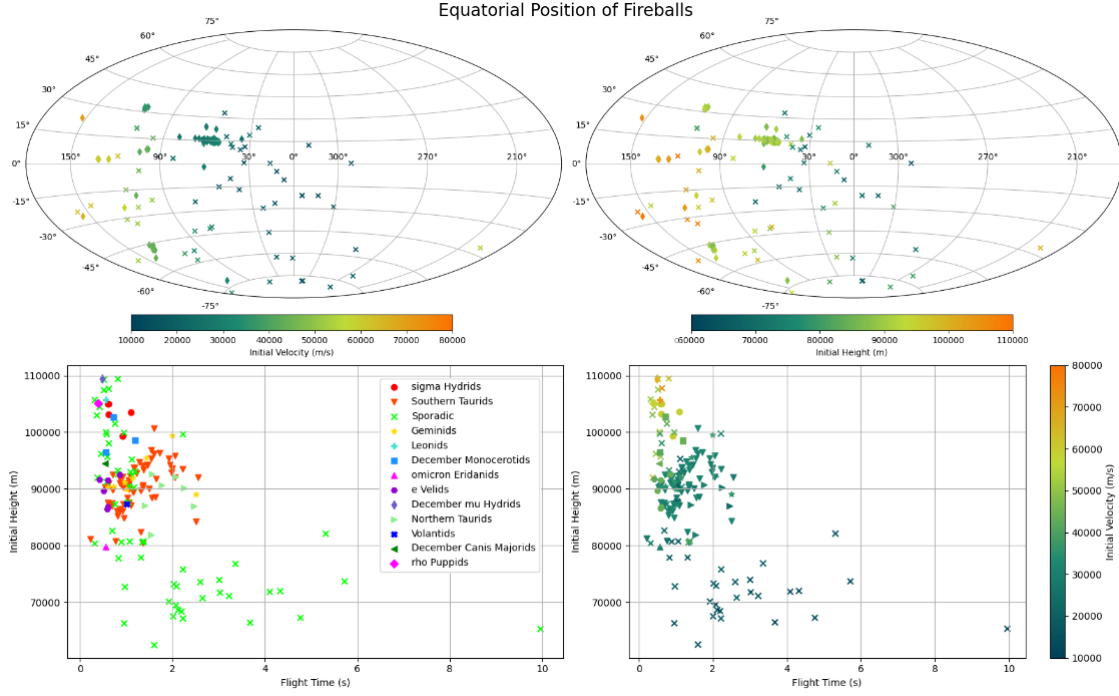


Figure 4. Shows an overview of some interesting physical parameters associated with each fireball and conclusions can be drawn more broadly of each meteor shower. The top panels show the incoming positions of fireballs with the colourbars indicating the initial velocity (m/s) on the left and the initial height (m) on the right, as the fireballs enter their bright flight phases. The sporadic fireballs are represented by the crosses, while shower members are represented by diamonds, Figure 3 can be used as a reference to indicate the appropriate shower. The two bottom panels show the bright flight time (sec) vs. the initial height (m) of the fireballs as they enter their bright flight phase. The bottom left panel shows this by differentiating meteor showers by marker style and colour, while the bottom right panel delineates the meteor showers by marker style with the colour representing the initial velocity (m/s) of the bright flight phase.

Table 2. Average colour-indices of each shower over the fireballs entire bright flight phase and for each shower at 75 km above the Earth from the data plotted in Figures 5 and 6. The December Monocerotid, omicron Eridanid, and rho Puppis showers were not included as they did not have the colour-index data to plot. The first three columns of data (Average Colour-Index Value) have the number of events plotted in the Events column in brackets, while the last three columns of data (Average Colour-Index at 75 km) show the number of events plotted in brackets within the columns. Showers with only one event plotted have no variance quoted, except for the Northern Taurids, where data was available for two of the seven events in the G-R colour-index. No events from the Leonids, December mu Hydrids, or December Canis Majorids passed through an altitude of 75km while in the bright flight phase.

Shower	Events	Average Colour-Index Value			Average Colour-Index at 75km		
		G-R	B-G	B-R	G-R	B-G	B-R
Sporadic	61 (30)	-0.09 ± 0.58	0.41 ± 0.78	0.35 ± 0.45	0.39 ± 0.76 (9)	-0.07 ± 0.98 (9)	0.31 ± 0.45 (12)
Southern Taurids	65 (23)	0.11 ± 0.58	0.17 ± 0.67	0.29 ± 0.35	-0.17 ± 0.31 (7)	0.54 ± 0.40 (7)	0.30 ± 0.23 (9)
Geminids	8 (7)	-0.17 ± 0.60	0.53 ± 0.89	0.36 ± 0.55	-0.58 ± 0.23 (3)	0.90 ± 0.36 (3)	0.32 ± 0.14 (3)
Northern Taurids	7 (1)	-1.40 ± 0.25	4.96	3.05	-0.80	4.60	3.80
e Velids	6 (4)	-0.09 ± 0.27	0.25 ± 0.37	0.16 ± 0.14	-0.46 ± 0.17 (3)	0.56 ± 0.16 (3)	0.10 ± 0.11 (3)
sigma Hydrids	5 (3)	0.09 ± 0.29	-0.08 ± 0.23	0.005 ± 0.059	-0.29	0.13	-0.16
Leonids	1 (1)	-0.16	0.57	0.41	-	N/A	-
December mu Hydrids	1 (1)	0.26	-0.05	0.20	-	N/A	-
Volantids	1 (1)	-2.59	2.98	-0.15	-1.63	1.66	0.03
December Canis Majorids	1 (1)	0.04	-0.09	-0.11	-	N/A	-

with the accompanying p-value, found that there was minimal to no significance in these results. A Bonferroni correction was employed

to account for multiple comparisons⁶.

⁶ P-values, Bonferroni corrections and the family-wise error rate can all be found in Table 1 and accompanying caption of the Appendix (5).

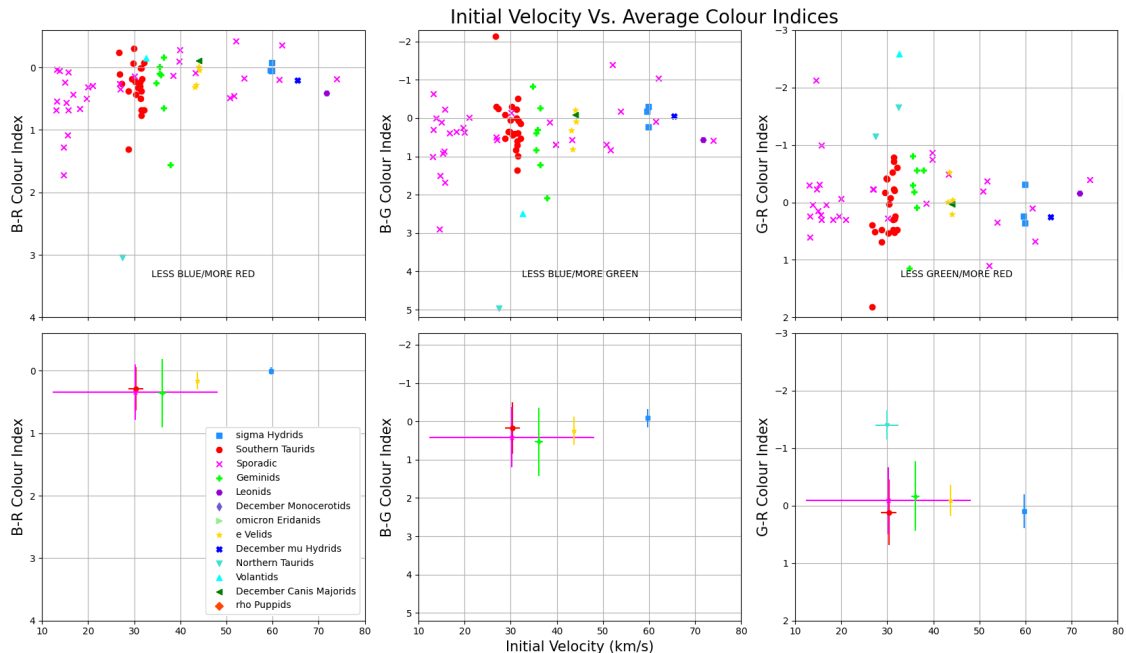


Figure 5. Shows the initial velocity (m/s) vs. the colour-indices (from left to right; B-R, B-G, and G-R). Both the top and bottom rows are displaying the same information, with the top row being the individual observations of each fireball in the shower and the second row being the average of each of the showers with standard deviations. Showers with only one observation are omitted from the bottom row as to not miss represent the data. Grouping of showers by velocity can easily be seen in the top row of panels, while the second row of panels better shows the difference between the average colour-index of each shower.

Within just the Taurid shower members, Figure 5 shows that the average value of the Southern (pale blue circles) and Northern (purple diamonds) Taurids are quite separate from each other. This is surprising given that these two showers share a radiant and are considered related, originally thought to be from the same parent body (Whipple & El-Din Hamid 1952), but more likely originating from a larger meteor complex (Devillepoix et al. 2021). This could account for differences in compositions, with these two showers originating from different parts of the same stream. Another potential explanation for this variance is the differences in the trajectory properties of these showers, where the slightly different entry velocities and radiants could be the dominant signal in the brightness of a fireball, compared to the geochemical properties of the meteoroids themselves.

In order to remove the effects of imaging biases due to the range of the fireball, we also plot the colour-indices when the fireball was at a height of 75 km. Not all fireballs pass through the 75 km plane and so fewer observations are available. The top row in each of Figures 5 and 6 show the variation in colour-index for shower material vs. sporadics. Although Figure 5 shows very little clustering, Figure 6 shows that sporadic events are capable of being significantly less green overall (high G-R, Low B-G, no preference in B-R). This could be an indicator of asteroidal material origins vs. cometary shower material, which would be of significant importance, as such differentiation is traditionally made based on strength profiles of a body (Kikwaya et al. 2011). However, this trend

is far more likely related to the velocity of the incoming fireball. The right column (G-R) of Figure 6 does support a trend with velocity, with fireballs slower than 20 km/s appearing far less green than their faster counterparts. This trend is seen faintly in the left column of this figure, but not apparent in the central column.

To further understand this, we plot the initial velocity of the fireballs in question at an altitude of 75 km against the colour-index measured at this time with a line of best fit through the data in Figure 7, with the shaded regions indicating the 95% confidence interval. The central panel of Figure 7 shows a similar dependence on velocity to that seen in Figure 4 of Hajdukova (1974), which indicates that, the lower the initial velocity of an incoming meteor, the bluer it becomes. Our fireball data seems to mirror this result for the B-G colour-index, which is the most comparable to the colour-index calculated in Hajdukova (1974). Hajdukova (1974) found that a meteor becomes bluer at a rate of 12-16 mmag per km/s for decreasing initial velocity. Our data indicates a rate of 23 ± 11 mmag per km/s. This value agrees with the trend suggested in literature within error, however, the error found is large enough that it degrades the statistical significance. Further investigation, with the complete data set is needed to more completely understand the relationship between colour-index and initial velocity. This could potentially be achieved by looking at the colour-index at different altitudes or looking at the absolute magnitude of the fireballs as opposed to the apparent magnitude. Initially, studying the fireballs at a set height was to attempt to remove potential bias due to the varying seeing distances through the atmosphere (caused by the

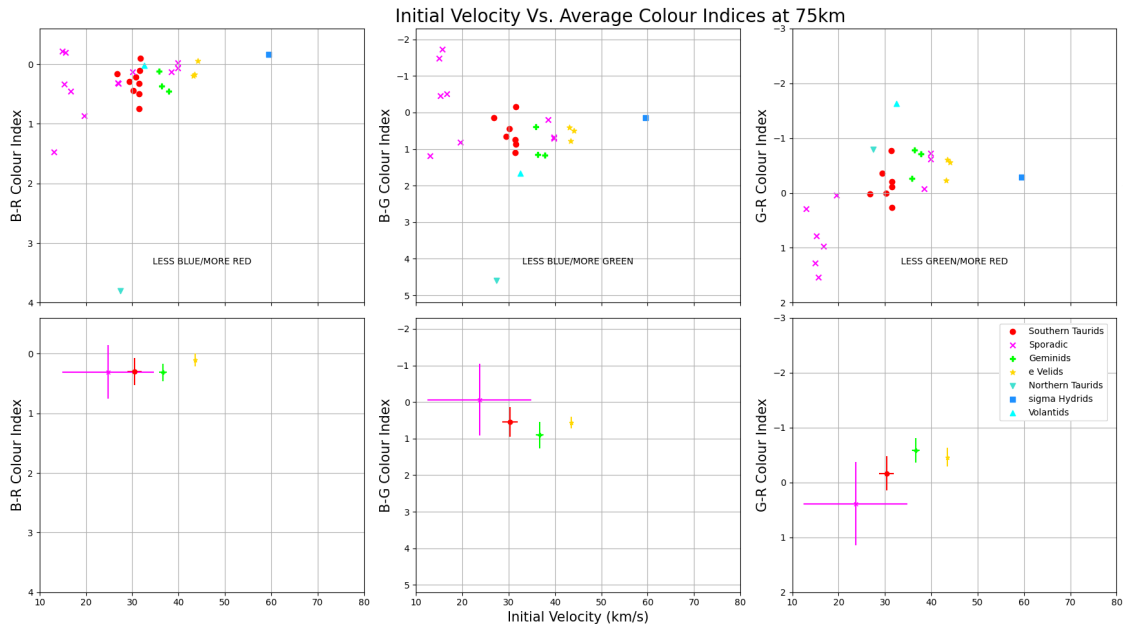


Figure 6. As in Figure 5 this figure shows the initial velocity (m/s) vs. the colour-indices (from left to right; B-R, B-G, and G-R), at a height of 75 km. It can be seen that not all fireballs pass through the 75 km plane and therefore there are fewer observations available. The data shows that sporadics are capable of being greener (lower G-R, and higher B-G) when compared with material from shower origins.

different observatory locations). This substitution of apparent for absolute magnitude would allow an analysis of a larger data set, not imposing the limit of fireballs that pass through a set altitude.

The left (B-R) and right (G-R) panels of Figure 7 indicate trends in the opposite direction, showing slower fireballs are redder in both the B-R, and G-R colour-indices at an altitude of 75 km at a rate of 17 ± 7 and 40 ± 5 mmag per km/s, respectively. From Borovička et al. (2005); Vojáček et al. (2015), it can be seen that the vast majority of contributions in the red band are from atmospheric effects due to the fireball ionising gases during the ablation process. This is potentially due to the longer time spent in the ablation phase, evidence for which can be seen in the bottom right panel of Figure 4. Again further analysis of a larger data set, and at varying altitudes, or with absolute magnitudes would be needed to gauge a stronger correlation between velocity and colour-index.

Further investigation is needed to confirm these findings. In addition, as meteor showers are a yearly occurrence this result may be due to a yearly bias not currently accounted for in this dataset. The dataset used in this study is a small sample of the total dataset available from the DFN, where data range from 2015 to present. This indicates that further analysis with a vastly larger dataset would be of benefit. This would allow a deeper investigation into each of the showers mentioned in this work on a year by year basis, as well as many other meteor streams visible to the Southern Hemisphere.

5 CONCLUSIONS

The Solar system's small bodies are a vital source of information about the origin and evolution of our planetary system. The Desert Fireball Network (DFN) observes the fireball events when debris and small bodies come through our atmosphere. Using their RGB images, photometry is explored as a low-cost alternative to a spectrometer, aiming to identify clustering of meteoroids from the same parent body.

This work makes use of a subset of data from the DFN, recorded in November and December 2015, to perform a pilot study of the RGB colours of 161 fireballs observed in that time. In doing so, we examine the similarities and differences between fireballs that are members of known meteor showers and the general sporadic background. This is intended as a preliminary study, to lay the groundwork for a larger more in-depth study utilising the entire DFN dataset.

When looking at colour-indices for fireballs at a comparable altitude of 75 km, we see that a velocity relation appears which matches a previous relationship found in Hajdukova (1974). This relationship indicates that slower fireballs appear bluer in the B-G colour-index, which is most comparable to the analogous B-V colour-index defined in Jacchia (1957) and used in Hajdukova (1974). This relationship could be used in the future as a proxy when velocity data is not available for an event or for when an event is only witnessed by a single camera. Further detrending needs to be performed to understand if these observations are the result of bias or a classifying feature of fireballs.

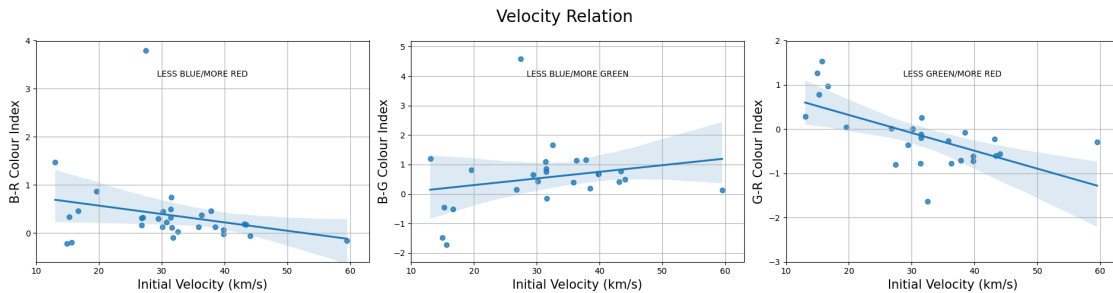


Figure 7. This figure shows the relationship between the velocity of the incoming fireball and the colour-indices (B-R, B-G, and G-R, from left to right), with the shaded regions of the plots being the 95% confidence interval. The central panel, which is our closest match to the B-V analogue calculated in Hajdukova (1974), can be seen to closely match the results found in the literature of $12\text{--}16$ mmag per km/s. From the data in the central panel it can be found that fireballs become bluer at a rate of 23 ± 11 mmag per km/s for decreasing initial velocity. Both the left (B-R) and right (G-R) panels show that a lower initial velocity is the cause of a redder fireball, at a rate of 17 ± 7 and 40 ± 5 mmag per km/s, respectively.

Our data reveals a tendency for the Southern Taurids to appear significantly less green and more red compared to the Northern Taurid members, despite being thought to share a common origin (Whipple & El-Din Hamid 1952). This incompatibility would indicate that there is a difference between these two Taurid streams. Given the small sample size of the Northern Taurids in this pilot study, this is likely to be an outlier. Nevertheless, it warrants further investigation.

This study demonstrates the potential of the data obtained by the DFN as a resource for investigating the similarities and differences between different meteor showers, but, like the work of Moorhead & Kingery (2020), is limited by the relatively small dataset used. In future work, we intend to expand this pilot study to cover data from all months of the calendar year, and from all years over which the DFN has been active.

In addition to directly comparing individual meteor showers using the entire dataset, we also intend to perform year-to-year comparisons for individual showers. The expanded dataset will also allow us to continue the investigation into the apparent differences in the Northern and Southern Taurids, sporadic and shower members, and any differences between ‘standard’ and ‘swarm’ years.

ACKNOWLEDGEMENTS

This research is supported by the Australian Research Council through the Linkage Infrastructure, Equipment, and Facilities program (LE170100106). The DFN receives institutional support from Curtin University and uses the computing facilities of the Pawsey Supercomputing Center. The DFN team would like to thank the hosts of all of the Fireball observatories whose data was used in this work. We respectfully acknowledge the traditional custodians of all lands throughout Australia, and recognise their continued cultural and spiritual connection to the land, waterways, cosmos, and community. We pay our deepest respects to all Elders, ancestors and descendants of the lands around our host institutions, and on which our cameras are situated. The authors would also like to express their sincere gratitude to the anonymous referee of this paper, whose suggestions help to significantly expand and improve our work.

MNRAS **000**, 1–11 (2023)

DATA AVAILABILITY

The data used in this study was accessed through the Desert Fireball Network. Subsequent data generated throughout this research can be accessed through request via the corresponding author.

REFERENCES

- Anderson S. L., et al., 2022, *ApJ*, **930**, L25
 Asher D. J., Bailey M. E., Emel’Yanenko V. V., 1999, *MNRAS*, **304**, L53
 Belton M. J. S., Morgan T. H., Samarasinha N. H., Yeomans D. K., 2011, Mitigation of Hazardous Comets and Asteroids
 Bland P. A., Artemieva N. A., 2006, *Meteoritics and Planetary Science*, **41**, 607
 Borovička J., Koten P., Spurný P., Boček J., Štork R., 2005, *Icarus*, **174**, 15
 Bus S. J., 1999, PhD thesis, Massachusetts Institute of Technology, Massachusetts, <https://dspace.mit.edu/handle/1721.1/9527>
 Campbell-Brown M. D., Borovička J., Brown P. G., Stokan E., 2013, *A&A*, **557**, A41
 Carlson R. W., Holland H. D., Turekian K. K., 2003, *Treatise on Geochemistry*, **2**, 568
 Cepelcha Z., Borovička J., Elford W. G., Revelle D. O., Hawkes R. L., Porubčan V., Šimek M., 1998, *Space Sci. Rev.*, **84**, 327
 DeMeo F., Binzel R. P., 2008, *Icarus*, **194**, 436
 DeMeo F. E., Binzel R. P., Slivan S. M., Bus S. J., 2009, *Icarus*, **202**, 160
 Devillepoix H. A. R., 2018, PhD thesis, Curtin University, Perth, Western Australia, <http://hdl.handle.net/20.500.11937/76001>
 Devillepoix H. A. R., et al., 2018, *Meteoritics and Planetary Science*, **53**, 2212
 Devillepoix H. A. R., et al., 2020, *Planetary and Space Science*, **191**, 105036
 Devillepoix H. A. R., et al., 2021, *The Planetary Science Journal*, **2**, 223
 Dworkin J. P., Osiris-Rex Team 2017, in XVIIIth International Conference on the Origin of Life. p. 4095
 Ganapathy R., Brownlee D. E., 1979, *Science*, **206**, 1075
 Grossman J., 2005, Meteoritical Bulletin Database, <https://www.lpi.usra.edu/meteor/>
 Hajdukova M., 1974, Bulletin of the Astronomical Institutes of Czechoslovakia, **25**, 365
 Horner J., Evans N. W., Bailey M. E., Asher D. J., 2003, *MNRAS*, **343**, 1057
 Horner J., Evans N. W., Bailey M. E., 2004a, *MNRAS*, **354**, 798
 Horner J., Evans N. W., Bailey M. E., 2004b, *MNRAS*, **355**, 321
 Horner J., et al., 2020, *PASP*, **132**, 102001
 Howie R., Paxman J., Bland P., Towner M., Cupak M., Sansom E., Devillepoix H., 2017, *Experimental Astronomy*, **43**, 1
 Jachia L. G., 1957, *AJ*, **62**, 358

- Jansen-Sturgeon T., Sansom E. K., Bland P. A., 2019, *Meteoritics and Planetary Science*, **54**, 2149
- Jenniskens P., 2004, *AJ*, **127**, 3018
- Jenniskens P., 2006, Meteor Showers and their Parent Comets
- Jenniskens P., et al., 2019, *Meteoritics & Planetary Science*, **54**, 699
- Kasuga T., Jewitt D., 2019, in Ryabova G. O., Asher D. J., Campbell-Brown M. J., eds., *Meteoroids: Sources of Meteors on Earth and Beyond*, p. 187
- Kikwaya J. B., Campbell-Brown M., Brown P. G., 2011, *A&A*, **530**, A113
- Kresák L., 1972, *Bulletin of the Astronomical Institutes of Czechoslovakia*, **23**, 1
- Levison H. F., Duncan M. J., 1994, *Icarus*, **108**, 18
- Love S. G., Brownlee D. E., 1993, *Science*, **262**, 550
- Mainzer A., et al., 2011, *ApJ*, **743**, 156
- Marsden B. G., 1973, *AJ*, **78**, 654
- McIntosh B. A., 1990, *Icarus*, **86**, 299
- Meier M. M. M., 2017, Meteorite Orbits .info, <https://www.meteoriteorbits.info/>
- Moorhead A. V., Kingery A., 2020, WGN, Journal of the International Meteor Organization, **48**, 193
- Murray C. D., Dermott S. F., 2000, *Solar System Dynamics*, doi:10.1017/CBO9781139174817.
- Nesvorný D., Jenniskens P., Levison H. F., Bottke W. F., Vokrouhlický D., Gounelle M., 2010, *ApJ*, **713**, 816
- Ocaña F., 2017, PhD thesis, Complutense University of Madrid, Spain
- Plane J. M. C., 2012, *Chemical Society Reviews*, **41**, 6507
- Radau R., 1896, *Bulletin Astronomique, Serie I*, **13**, 300
- Rubin A. E., Grossman J. N., 2010, *Meteoritics and Planetary Science*, **45**, 114
- Sansom E. K., Bland P., Paxman J., Towner M., 2015, *Meteoritics and Planetary Science*, **50**, 1423
- Sansom E. K., Rutten M. G., Bland P. A., 2017, *The Astronomical Journal*, **153**, 87
- Sansom E. K., et al., 2019, *The Astrophysical Journal*, **885**, 115
- Sansom E. K., et al., 2020, *Meteoritics & Planetary Science*, **55**, 2157
- Shober P. M., et al., 2021, *Planetary Science Journal*, **2**, 98
- Soja R. H., et al., 2019, *A&A*, **628**, A109
- Sugita S., et al., 2020, in European Planetary Science Congress. pp EPSC2020-995
- Tholen D. J., 1984, PhD thesis, The University of Arizona, Arizona, <https://repository.arizona.edu/handle/10150/187738>
- Towner M. C., et al., 2020, *Publications of the Astronomical Society of Australia*, **37**, e008
- Vojáček V., Borovička J., Koten P., Spurný P., Štork R., 2015, *Astronomy and Astrophysics*, **580**, A67
- Whipple F. L., 1983, *IAU Circ.*, **3881**, 1
- Whipple F. L., El-Din Hamid S., 1952, *Helwan Institute of Astronomy and Geophysics Bulletins*, **41**, 3
- Williams I. P., Wu Z. D., 1994, *MNRAS*, **269**, 524
- Wu Z., Williams I. P., 1993, *MNRAS*, **264**, 980
- Ye Q., Jenniskens P., 2022, arXiv e-prints, p. arXiv:2209.10654
- Yeomans D. K., 1981, *Icarus*, **47**, 492
- Yeomans D. K., Yau K. K., Weissman P. R., 1996, *Icarus*, **124**, 407
- Yoshikawa M., Kawaguchi J., Fujiwara A., Tsuchiyama A., 2021, in Longobardo A., ed., *Sample Return Missions*. Elsevier, pp 123–146, doi:<https://doi.org/10.1016/B978-0-12-818330-4.00006-9>, <https://www.sciencedirect.com/science/article/pii/B9780128183304000069>

5

This paper has been typeset from a $\text{\TeX}/\text{\LaTeX}$ file prepared by the author.

Table 1. These are the p-values from the Welch's t-test's performed on the data represented in Figure 5. The Bonferroni correction was calculated to be 0.005 for the B-R and B-G colour-indices, and 0.003 for the G-R colour-index. The difference in these corrections is due to the availability of extra data in the G-R colour-index of the Northern Taurid stream. The use of the Bonferroni correction allows the family-wise error rate to remain constant, otherwise, a higher false positive rate would be introduced throughout the sample. It can be seen from this table that there are only two instances of a difference in means passing a Welch's t-test, seen bolded in the sigma Hydrids column (and in the same row).

Shower	S. Taurids			Sporadic			Geminids			e Velids			sigma Hydrids			N. Taurid
	B-R	B-G	G-R	B-R	B-G	G-R	B-R	B-G	G-R	B-R	B-G	G-R	B-R	B-G	G-R	G-R
Southern Taurids	1.0	1.0	1.0	0.6	0.24	0.23	0.77	0.38	0.33	0.27	0.77	0.33	0.004	0.29	0.93	0.06
Sporadic	0.6	0.24	0.23	1.0	1.0	1.0	0.96	0.77	0.77	0.13	0.56	0.98	0.001	0.06	0.5	0.79
Geminids	0.77	0.38	0.33	0.96	0.77	0.77	1.0	1.0	1.0	0.43	0.52	0.8	0.17	0.16	0.45	0.03
Northern Taurids	nan	nan	0.06	nan	nan	0.08	nan	nan	0.03	nan	nan	0.06	nan	nan	0.03	1.0
e Velids	0.27	0.77	0.33	0.13	0.55	0.98	0.43	0.52	0.8	1.0	1.0	1.0	0.16	0.27	0.52	0.06
sigma Hydrids	0.004	0.29	0.93	0.001	0.06	0.5	0.17	0.16	0.45	0.16	0.27	0.52	1.0	1.0	1.0	0.35

3.3 ASSOCIATED PRESENTATIONS

3.3.1 *SEPTEMBER 2022, AUSTRALIAN SPACE RESEARCH CONFERENCE - ORAL PRESENTATION*

Title: The Colour of Falling Rocks

Authors: Johnson, Chris; Sansom, Ellie; Horner, Jonti; Devillepoix, Hadrien; Towner, Martin; Wright, Duncan; Carter, Brad

Abstract:

Since 2005 the Desert Fireball Network (DFN) has been collecting data on meteors that have appeared throughout the Australian sky. This study aims to further understand and improve the classification of meteors and meteorites using fireball data taken by cameras in the DFN. Currently, little work has been carried out into the classification of meteors based primarily on their colours. The DFN offers one of the largest catalogs of meteor photometric colour, magnitudes, and trajectory information in the world, which makes the DFN an unparalleled resource. This study has allowed the curation of information from multiple sources and further analysis to be undertaken. From preliminary results, it appears that the Southern Taurid meteor shower may be both more red and less green in visual appearance when compared to other showers. Overall, this has proved to be an interesting new avenue for the classification of meteor showers, and we plan to investigate further through our access to more data from the wider DFN collaboration.

4

ANALYSIS AND DISCUSSION

4.1 UNDERSTANDING THE DATA

To understand how the data is collected and analysed, I was given access to some archival data from November and December of 2015, featuring fireballs from several larger meteor streams (Northern and Southern Taurids, Geminids, and Leonids), along with many minor streams (see Table 1 of the Todd et al. (2023) in Chapter 3 for full list), and a large proportion of sporadic fireballs. The data consisted of 229 separate events, most witnessed by multiple cameras, totaling 597 individual observations. This has allowed 383 observations from 161 events to be analysed with the full suite of the Desert Fireball Network (DFN) analysis packages. The observations which failed the preliminary data quality tests were a result of various timing issues. These issues could stem from a lack of data, due to smaller fireballs (either fainter or shorter duration), weather, or other visual obstructions, like the Moon (which causes saturation of the sensors, e.g. seen in Figure 2.4).

DN151228_01_Wooleen Magnitude and Colour-Indices Comparison

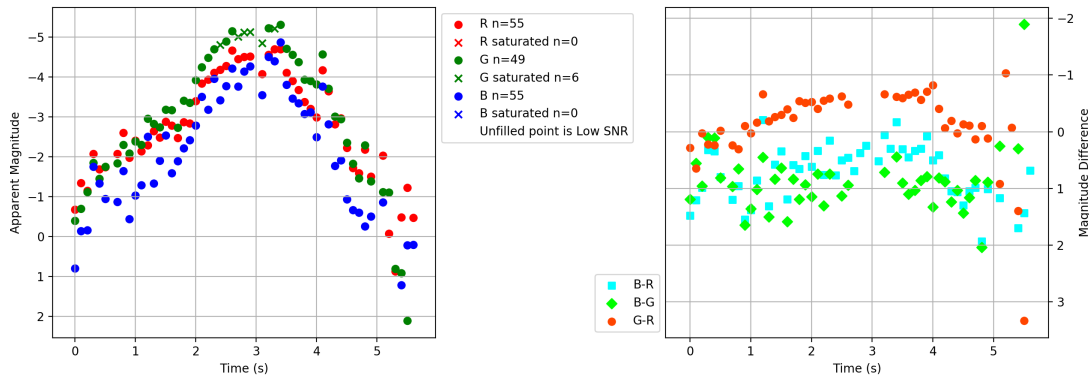


Figure 4.1: The left panel shows the apparent magnitude for the duration of the fireball’s bright flight. The right panel shows a plot of the colour-indices. The small gap in the centre of the colour-index plot is due to the saturation of the green colour channel, which can be seen represented by crosses in the left panel, indicating the sensor was saturated by the amount of light in that colour band. This figure is produced from data gained from a fireball observed on the 28th of December 2015, from the Wooleen observatory in Western Australia.

With access to the DFN software package (freely available on GitHub¹) and historical data, I have been able to gain an understanding of the code, which has allowed me to combine the data in a more complete catalog. Previously, the triangulation data and the visual data were in different files, which I have consolidated into one, to aid in future analysis. I have also made adjustments to the data files to allow easier access to key values for further analysis, such as peak magnitudes in each colour channel and the timing of these occurrences. I have constructed a side-by-side plot of apparent magnitude and the colour-indices to help with comparisons of different events (example seen in Figure 4.1).

As the next step of this analysis process, I have combined the observations from the different cameras for each event to have a singular overall plot of fireball apparent magnitude and colour-indices over time. This can be seen in Figure 4.2, with data gathered from five observatories in South Australia; Mulgathing, Ingomar, Baton, Mount

¹<https://github.com/desertfireballnetwork>

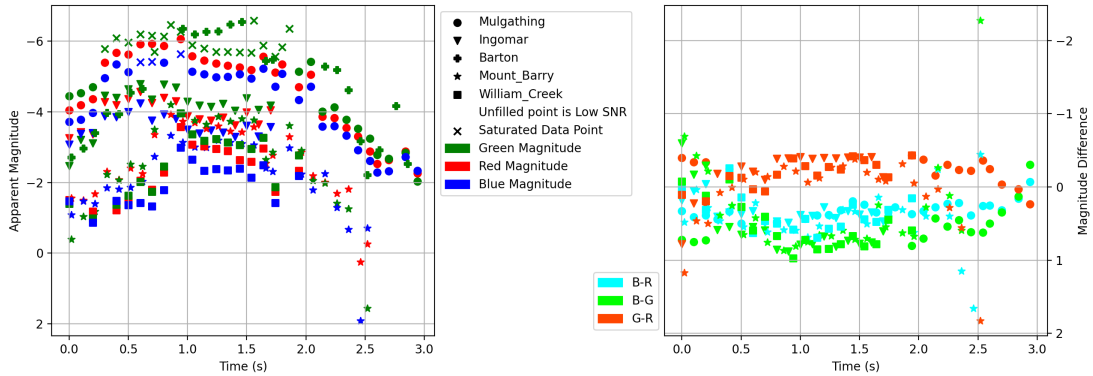


Figure 4.2: This figure shows an example of all observations from a single event in one graph. In the left panel, the apparent magnitude of the RGB colour channels can be seen. Each station is represented by a different marker, with five in total for this event. Data from Mulgathing (circle), Ingomar (inverted triangle), Barton (plus), Mount Barry (star), and William Creek (square) can be seen, with the colours representing the colour channel of the data (red, green, or blue). In the right panel, the available colour-indices can be seen (B-R, B-G, and G-R), using the same markers for each observation. This figure was produced with data gathered from the five observatories listed in South Australia from a fireball on the 5th of November 2015.

Barry, and William Creek. No colour-indices could be calculated from the data gained from the Barton observatory (in Figure 4.2), as only the green channel possessed a high enough signal-to-noise ratio. The left panel demonstrates the vast differences in apparent magnitude caused by local weather and observing distance. It can also be seen that despite these differences in apparent magnitude, the colour-indices mesh together nicely, as seen in the right panel of Figure 4.2. This demonstrates the invariant nature of colour-indices and therefore their comparability despite being measured from different locations under different conditions.

4.2 COLOUR-INDICES

Classifying fireballs via their initial velocity or height of the bright flight phase, or their radiants is not the aim of this study, merely an interesting and important cross-check to identify potential special cases. To further this investigation I calculated the colour-

indices (B-R, B-G, and G-R) for the observed fireballs and the average values for each shower. For a more in-depth discussion, see the associated Figure 5 and Table 1 of my paper, Todd et al. (2023), in Chapter 3 of this text (also including the table in the appendix).

In an attempt to remove some effects of imaging bias due to range (distance from the observatory to the fireball), I investigated the colour-indices at a fixed height. I chose an altitude of 75 km as it has the most amount of viable fireballs passing through it. Figure 6 and Table 2 in my paper (see Chapter 3) show this. Figures 4.3 and 4.4 were plotted to assess if any insights could be gained about the color-indices from shower groupings in equatorial co-ordinates. Similarities are seen in members of the same shower, however, these figures serve more to highlight outliers rather than gaining any new information. Perhaps with more events in the data, these figures will be of more assistance. They do still show that the sporadic fireballs within the sample are more variable than shower members, which is further confirmed upon viewing the data in Table 2 of my paper (see Chapter 3). In particular the last three columns, with the variance of the sporadic colour-indices being more than double that of showers in some cases.

Figure 6 in my paper (see Chapter 3) indicates a trend between colour-index and initial velocity. To investigate this further I plotted the initial velocity vs. the colour-index with a line of best fit, see Figure 7 of my paper. Figures 5 and 6 from my paper produce interesting results, however, the significance of these results must be viewed with tentative success given the variance seen in the data (plotted in Figures 5 and 6, and stated in Tables 1 and 2 of my paper). The variance could be due to the low sample size, which would improve with the addition of the complete data set observed by the DFN. The DFN has been observing the Australian skies since 2015. The dataset I have been granted access to is only for a two month period between November and December 2015. The complete DFN data set is approximately ten times this size and would further investigations into these trends found in this sample.

Or perhaps these differences are attributed to the differing trajectory properties of these showers. The trajectory properties (velocity, angle, etc.) of a meteor are seen to be the dominant signal received from a fireball, compared with the geochemical properties of the meteors themselves. The results found in this pilot study suffer from a small sample size, which reduces the statistical significance of the emerging trends found. A larger sample size will allow for further investigation, increasing the statistical significance of the current result, and open new avenues of investigation.

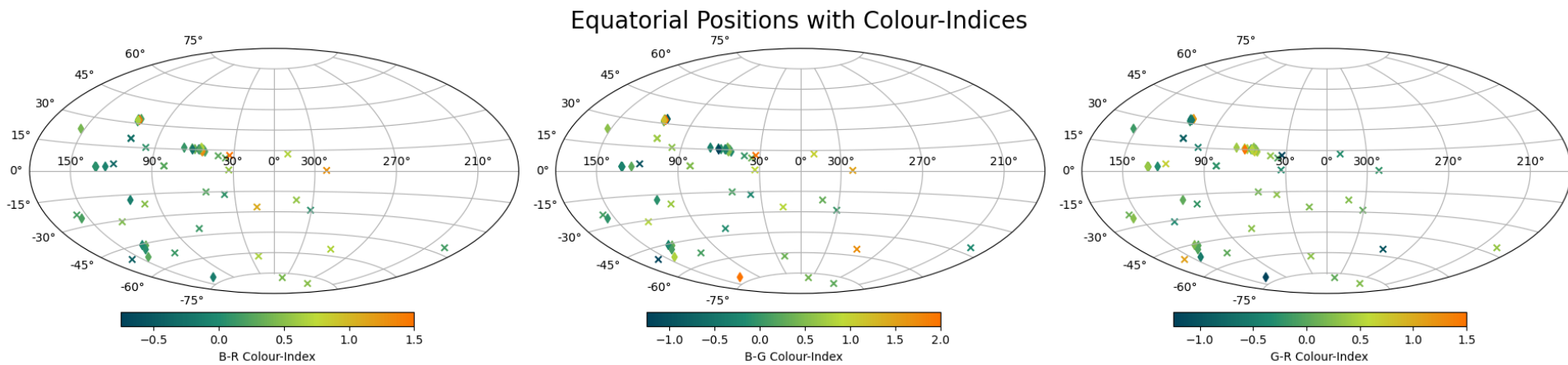


Figure 4.3: Shows the initial equatorial positions of available fireballs with the colourbars indicating the average colour-index (from left to right: B-R, B-G, and G-R) of the entire bright flight phase. From Figure 4.3, it can be noted that some fireballs fall outside of the quoted range, these instances are represented as the colours at the extremities of the colourbars. Figure ?? can be used as a reference to assist in locating specific showers. In this figure shower members are plotted as diamonds, while the crosses represent the sporadic data set.

Equatorial Positions with Colour-Indices at 75km

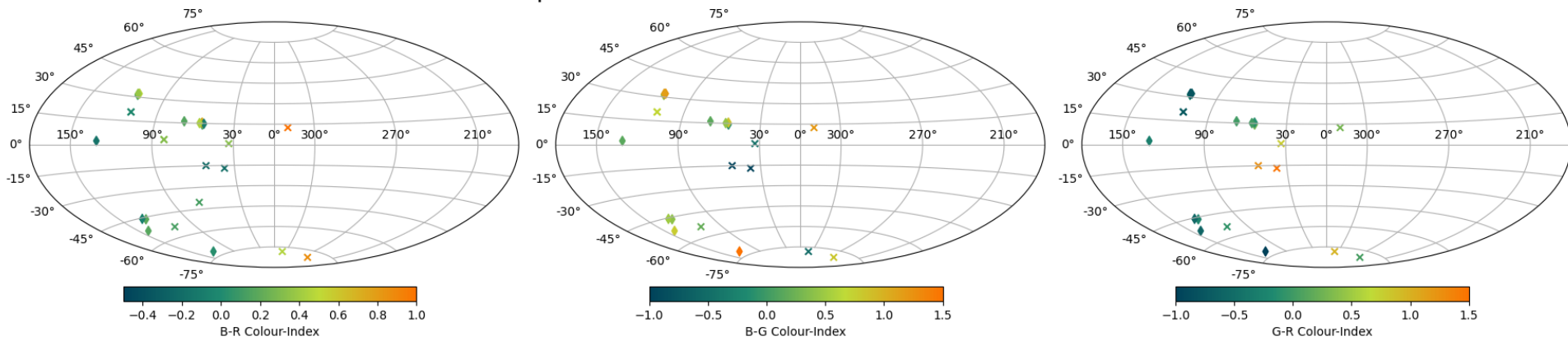


Figure 4.4: Shows the initial equatorial position of available fireballs which pass through an altitude of 75km, with the colourbar indicating the colour-index (from left to right: B-R, B-G, and G-R) at this altitude. Fireballs with a colour-index outside the colourbar range are represented by the extremity colours of the associated colourbar. Figure ?? can be used as a reference to assist in locating specific showers. As with Figure 4.3 shower members are plotted as diamonds, while the crosses represent the sporadic data set.

5

QUEENSLAND NETWORK DEPLOYMENT AND CONCLUSIONS

5.1 EASTERN NETWORK UPDATE

The Desert Fireball Network (DFN) began mass deployment of observatories in 2014, currently, there are more than 50 observatories across Australia (Devillepoix et al., 2020). As a secondary part of my project, I was tasked with setting up the North-Eastern division of the DFN. Excellent progress has been made, with the deployment of one additional DFN camera at Mt Kent Observatory, and plans to install a second in Glen Aplin in the coming months.

A photograph of the installation at the Mount Kent Observatory can be seen in the

right panel of Figure 2.2 in Section 2.1. This particular setup is rooftop mounted, with main power connection, as opposed to the traditional setup seen in Figure 2.1 which is completely autonomous. The rooftop setup was chosen over the traditional setup for geographical reasons and cost efficiency. The Mount Kent Observatory is already home to many ground-based telescopes used for other astronomical research at USQ and other universities. The site was chosen for ease of access for both installation and upkeep purposes. The camera is currently operational, however, it has not been connected to the rest of the DFN as it is pending IT approval.

The second site currently chosen is a private property in Glen Aplin, whose owner has agreed to house a completely autonomous setup (like the one seen in Figure 2.1 of Section 2.1). It will sit in a paddock alongside another privately owned telescope. This site was chosen to allow maximum coverage for the expansion of the network, as well as ease of access for both installation and upkeep purposes. The site is located approximately 100km south of the Mount Kent observatory. This distance between the two observatories sits well within the 150km limit of camera spacing, whilst still being far enough away to gain maximal coverage. The camera for this installation is currently awaiting final setup and site installation owing to several organisational factors and time constraints. It is hoped that these issues can be resolved soon. It is looking likely that this site will be operational within the next few months weather permitting.

5.2 CONCLUSIONS

There is a vast menagerie of information locked away in the Solar system's small bodies, which may hold clues to the origins and evolution of the planetary systems found within. In an ideal world, we would be able to visit large numbers of those objects, collect samples, and return them to the Earth for laboratory study. However, such sample-return missions are hugely expensive, and only return relatively small amounts of material to Earth. Fortunately, the Solar system provides us with a natural delivery mechanism for fragments of asteroids and comets - the constant flux of material en-

tering Earth's atmosphere, producing meteors and fireballs, and sometimes dropping meteorites.

The Desert Fireball Network (DFN) was set up to catalogue this activity, and to allow researchers to quickly locate and recover any meteorites that fall in the regions covered by the network's all-sky cameras. By observing fireballs from multiple locations simultaneously, it allows researchers to triangulate the paths of their flight through the atmosphere, and to predict the locations at which any resultant debris will fall to Earth. In the process, the DFN gathers a vast amount of data in the form of all-sky images, leading to it recording an ever-growing dataset of observational data for fireballs in the sky above Australia.

In this study I make use of a subset of data from the DFN, recorded in November and December 2015, to undertake a detailed pilot study to establish if RGB (red, green, and blue) colour of fireballs could be used to aid in the classification of meteors. It was shown by Moorhead and Kingery (2020) that the measurement of RGB colour alone could be used to loosely classify iron-type meteors. The ability to classify meteors by colour alone is a relatively inexpensive and easy way to gain information on the composition and nature of fragments of larger objects. This allows us to learn about the properties of the meteoroid's parent bodies, taking advantage of observations of notoriously serendipitous events. Such observations could potentially be used to differentiate between sporadic and shower meteors, allow the identification of meteors that appear to share a common origin, and provide tighter constraints on the physical parameters of the meteoroids and their parent bodies from single observations.

Hajdukova (1974) found the emergence of a trend between colour-index and velocity. Their data indicated that slower meteors appear bluer in the B-V colour-index defined in Jacchia (1957). This colour-index is most comparable to the B-G colour-index defined in my work. This relationship between colour-index and velocity could allow for shower associations to be proposed or confirmed from fireball events only witnessed

by single cameras.

The data in this study yielded observations of 229 unique fireball events across the network, with 161 of them possessing RGB data. During the time span of data collection, a number of major and minor meteor showers are active, and the dataset used here contains representatives of several showers, including the Northern and Southern Taurids and the Geminids. Section 4.1 discusses this and explains the steps made to organise the data, by combining observations from the same event and plotting these results (Figures 4.1 and 4.2). Section 4.1 and my paper in Chapter 3 also discuss the physical parameters that allow for shower determination.

Section 4.2 discusses the calculation of the colour-indices. Figure 5 in my paper (seen in Chapter 3) reveals the tendency for Southern Taurids to be overall less green (high G-R, low B-G) than other meteor showers and the sporadics in this dataset. Upon further investigation, it was found that this result lacks statistical significance, potentially due to the small size of the data set. It is hoped that with access to the complete DFN archival dataset this could be investigated further, as it could enable differentiation between the Southern Taurids and other showers. This figure also shows that the Northern and Southern Taurids appear disjoint from one another, despite being thought to originate from the same parent body (Whipple and El-Din Hamid, 1952). Given the singular observation from the Northern Taurids in the sample, this could likely be an outlier, however, it warrants further investigation.

Figure 6 of my paper (seen in Chapter 3) shows that sporadic fireballs are capable of being significantly less green (high G-R, low B-G), compared with known shower members. This is thought to be linked to the velocity of an incoming fireball, which can be seen in Figure 7 of my paper. This figure shows that the B-G colour-index becomes bluer with decreasing incoming velocity at a rate of 23 ± 11 mmag per km/s. This agrees with results found in Hajdukova (1974). It is hoped that the large error can be resolved with access to the complete DFN dataset. Both B-R and G-R show trends indicating

slower fireballs appear redder at a rate of 17 ± 7 and 40 ± 5 mmag per km/s, respectively. This is potentially due to the extended period of time in the ablation phase, allowing more ionisation of gases around the fireball as it traverses the atmosphere. If a reliable velocity relation can be established it could allow colour to be used as a proxy when velocity data is unavailable. This could also potentially allow shower associations to be proposed or confirmed through single camera observations when trajectory data is unavailable.

These conclusions must be investigated further as the sample size of the data is not large enough to be certain, however, it does demonstrate the potential for using colour variations to establish trends within the data. In the next steps of this project, I plan to expand the current data set to include the complete set of archival data in the DFN archives. The DFN archival data set is approximately ten times large than the one presented in this work and will allow the continuation of this study.

The expanded dataset will allow me to remove some of the bias associated with the observation location of the fireballs, with data from the entire year which encompasses the shifting Right Ascension and Declination throughout the year. It will allow me to compare individual showers from year-to-year, and investigate any differences between 'standard' and 'swarm' years of known showers. In addition, it will allow me to continue the investigation into the use of colour as a proxy for velocity, the apparent differences between the Northern and Southern Taurids, and if colour could be an indicator for asteroidal (sporadic) vs. cometary (showers) material.

REFERENCES

Note that the references presented here are for Chapters 1, 2, 4 and 5. References for the papers included in Chapters 3 are included in the references sections of the papers.

Abbott, T. M. C., Abdalla, F. B., Allam, S., Amara, A., Annis, J., Asorey, J., Avila, S., Ballester, O., Banerji, M., Barkhouse, W., Baruah, L., Baumer, M., Bechtol, K., Becker, M. R., Benoit-Lévy, A., Bernstein, G. M., Bertin, E., Blazek, J., Bocquet, S., Brooks, D., Brout, D., Buckley-Geer, E., Burke, D. L., Busti, V., Campisano, R., Cardiel-Sas, L., Carnero Rosell, A., Carrasco Kind, M., Carretero, J., Castander, F. J., Cawthon, R., Chang, C., Chen, X., Conselice, C., Costa, G., Crocce, M., Cunha, C. E., D'Andrea, C. B., da Costa, L. N., Das, R., Daues, G., Davis, T. M., Davis, C., De Vicente, J., DePoy, D. L., DeRose, J., Desai, S., Diehl, H. T., Dietrich, J. P., Dodelson, S., Doel, P., Drlica-Wagner, A., Eifler, T. F., Elliott, A. E., Evrard, A. E., Farahi, A., Fausti Neto, A., Fernandez, E., Finley, D. A., Flaugher, B., Foley, R. J., Fosalba, P., Friedel, D. N., Frieman, J., García-Bellido, J., Gaztanaga, E., Gerdes, D. W., Giannantonio, T., Gill, M. S. S., Glazebrook, K., Goldstein, D. A., Gower, M., Gruen, D., Gruendl, R. A., Gschwend, J., Gupta, R. R., Gutierrez, G., Hamilton, S., Hartley, W. G., Hinton, S. R., Hislop, J. M., Hollowood, D., Honscheid, K., Hoyle, B., Huterer, D., Jain, B., James, D. J., Jeltama, T., Johnson, M. W. G., Johnson, M. D., Kacprzak, T., Kent, S., Khullar, G., Klein, M., Kovacs, A., Koziol, A. M. G., Krause, E., Kremin, A., Kron, R., Kuehn, K., Kuhlmann, S., Kuropatkin, N., Lahav, O., Lasker, J., Li, T. S., Li, R. T., Liddle, A. R., Lima, M., Lin, H., López-Reyes, P., MacCrann, N., Maia, M. A. G., Maloney, J. D., Manera, M., March, M., Marriner, J., Marshall, J. L., Martini, P., McClintock, T., McKay, T., McMahon, R. G., Melchior, P., Menanteau, F., Miller, C. J., Miquel, R., Mohr, J. J., Morganson, E., Mould, J., Neilsen, E., Nichol, R. C., Nogueira, F., Nord, B., Nugent, P., Nunes, L., Ogando, R. L. C., Old, L., Pace, A. B., Palmese, A., Paz-Chinchón, F., Peiris, H. V., Percival, W. J., Petravick, D., Plazas, A. A., Poh, J., Pond, C., Porredon, A., Pujol, A., Refregier, A., Reil, K., Ricker, P. M., Rollins, R. P., Romer, A. K.,

Roodman, A., Rooney, P., Ross, A. J., Rykoff, E. S., Sako, M., Sanchez, M. L., Sanchez, E., Santiago, B., Saro, A., Scarpine, V., Scolnic, D., Serrano, S., Sevilla-Noarbe, I., Sheldon, E., Shipp, N., Silveira, M. L., Smith, M., Smith, R. C., Smith, J. A., Soares-Santos, M., Sobreira, F., Song, J., Stebbins, A., Suchyta, E., Sullivan, M., Swanson, M. E. C., Tarle, G., Thaler, J., Thomas, D., Thomas, R. C., Troxel, M. A., Tucker, D. L., Vikram, V., Vivas, A. K., Walker, A. R., Wechsler, R. H., Weller, J., Wester, W., Wolf, R. C., Wu, H., Yanny, B., Zenteno, A., Zhang, Y., Zuntz, J., DES Collaboration, Juneau, S., Fitzpatrick, M., Nikutta, R., Nidever, D., Olsen, K., Scott, A. and NOAO Data Lab 2018, 'The dark energy survey: Data release 1', *The Astrophysical Journal Supplement Series*, vol. 239, no. 2, pp. 18.

Anderson, S. L., Bland, P. A., Towner, M. C. and Paxman, J. P., 2019, Utilizing drones and machine learning for meteorite searching and recovery, *in* '50th Annual Lunar and Planetary Science Conference', Lunar and Planetary Science Conference, pp. 2426.

Anderson, S. L., Towner, M. C., Fairweather, J., Bland, P. A., Devillepoix, H. A. R., Sansom, E. K., Cupák, M., Shober, P. M. and Benedix, G. K. 2022, 'Successful Recovery of an Observed Meteorite Fall Using Drones and Machine Learning', *The Astrophysical Journal Letters*, vol. 930, no. 2, pp. L25.

Asher, D. J. 1999, 'The Leonid meteor storms of 1833 and 1966', *Monthly Notices of the Royal Astronomical Society*, vol. 307, no. 4, pp. 919–924.

Asher, D. J., Bailey, M. E. and Emel'Yanenko, V. V. 1999, 'Resonant meteoroids from Comet Tempel-Tuttle in 1333: the cause of the unexpected Leonid outburst in 1998', *Monthly Notices of the Royal Astronomical Society*, vol. 304, no. 4, pp. L53–L56.

Bayer, B. E., 1976, 'Color imaging array'.

Binzel, R. P. and Xu, S. 1993, 'Chips off of asteroid 4 vesta: Evidence for the parent body of basaltic achondrite meteorites', *Science*, vol. 260, no. 5105, pp. 186–191, <https://www.science.org/doi/abs/10.1126/science.260.5105.186>

Bland, P. A. and Artemieva, N. A. 2006, 'The rate of small impacts on Earth', *Meteoritics and Planetary Science*, vol. 41, no. 4, pp. 607–631.

Borovicka, J. 1990, 'The comparison of two methods of determining meteor trajectories from photographs', *Bulletin of the Astronomical Institutes of Czechoslovakia*, vol. 41, pp. 391.

Borovička, J. 1993, 'A fireball spectrum analysis', *Astronomy and Astrophysics*, vol. 279, no. 2, pp. 627–645.

Borovička, J., Koteš, P., Spurný, P., Boček, J. and Štork, R. 2005, 'A survey of meteor spectra and orbits: evidence for three populations of Na-free meteoroids', *Icarus*, vol. 174, no. 1, pp. 15–30.

Brearley, A. and Jones, R. (2019), *Chondritic meteorites*, https://www.researchgate.net/publication/331162057_Chondritic_meteorites

Brown, M. E., Trujillo, C. and Rabinowitz, D. 2004, 'Discovery of a Candidate Inner Oort Cloud Planetoid', *The Astrophysical Journal*, vol. 617, no. 1, pp. 645–649.

Buder, S., Sharma, S., Kos, J., Amarsi, A. M., Nordlander, T., Lind, K., Martell, S. L., Asplund, M., Bland-Hawthorn, J., Casey, A. R., De Silva, G. M., D'Orazi, V., Freeman, K. C., Hayden, M. R., Lewis, G. F., Lin, J., Schlesinger, K. J., Simpson, J. D., Stello, D., Zucker, D. B., Zwitter, T., Beeson, K. L., Buck, T., Casagrande, L., Clark, J. T., Čotar, K., Da Costa, G. S., de Grijs, R., Feuillet, D., Horner, J., Kafle, P. R., Khanna, S., Kobayashi, C., Liu, F., Montet, B. T., Nandakumar, G., Nataf, D. M., Ness, M. K., Spina, L., Tepper-García, T., Ting(), Y.-S., Traven, G., Vogrinčič, R., Wittenmyer, R. A., Wyse, R. F. G., Žerjal, M. and Collaboration, G. 2021, 'The GALAH+ survey: Third data release', *Monthly Notices of the Royal Astronomical Society*, vol. 506, no. 1, pp. 150–201, <https://doi.org/10.1093/mnras/stab1242>

Bus, S. J. (1999), *Compositional Structure in the Asteroid Belt: Results of a Spectroscopic Survey*, PhD thesis, Massachusetts Institute of Technology, Massachusetts, <https://dspace.mit.edu/handle/1721.1/9527>

Carroll, B. W. and Ostlie, D. A. 2007, *An Introduction to Modern Astrophysics*, 2nd (international) edn.

Ceplecha, Z. 1959, 'On the colour index of meteors', *Bulletin of the Astronomical Institutes of Czechoslovakia*, vol. 10, pp. 39.

Ceplecha, Z. 1987, 'Geometric, dynamic, orbital and photometric data on meteoroids from photographic fireball networks', *Bulletin of the Astronomical Institutes of Czechoslovakia*, vol. 38, pp. 222.

Ceplecha, Z., Borovička, J., Elford, W. G., Revelle, D. O., Hawkes, R. L., Porubčan, V. and Šimek, M. 1998, 'Meteor Phenomena and Bodies', , vol. 84, pp. 327–471.

Citron, R. I., Jenniskens, P., Watkins, C., Sinha, S., Shah, A., Raissi, C., Devillepoix, H. and Albers, J. 2021, 'Recovery of meteorites using an autonomous drone and machine learning', *Meteoritics and Planetary Science*, vol. 56, no. 6, pp. 1073–1085. , <https://onlinelibrary.wiley.com/doi/abs/10.1111/maps.13663>

Colas, F., Zanda, B., Bouley, S., Jeanne, S., Malygoyre, A., Birlan, M., Blanpain, C., Gattaccecchia, J., Jorda, L., Lecubin, J., Marmo, C., Rault, J. L., Vaubaillon, J., Vernazza, P., Yohia, C., Gardiol, D., Nedelcu, A., Poppe, B., Rowe, J., Forcier, M., Koschny, D., Trigo-Rodriguez, J. M., Lamy, H., Behrend, R., Ferrière, L., Barghini, D., Buzzoni, A., Carbognani, A., Di Carlo, M., Di Martino, M., Knapic, C., Londero, E., Pratesi, G., Rasetti, S., Riva, W., Stirpe, G. M., Valsecchi, G. B., Volpicelli, C. A., Zorba, S., Coward, D., Drolshagen, E., Drolshagen, G., Hernandez, O., Jehin, E., Jobin, M., King, A., Nitschelm, C., Ott, T., Sanchez-Lavega, A., Toni, A., Abraham, P., Affaticati, F., Albani, M., Andreis, A., Andrieu, T., Anghel, S., Antaluca, E., Antier, K., Appéré, T., Armand, A., Ascione, G., Audureau, Y., Auxepaules, G., Avoscan, T., Baba Aissa, D., Bacci, P., Bu, O., Baldini, R., Baldo, R., Balestrero, A., Baratoux, D., Barbotin, E., Bardy, M., Basso, S., Bautista, O., Bayle, L. D., Beck, P., Bellitto, R., Belluso, R., Benna, C., Benammi, M., Beneteau, E., Benkhaldoun, Z., Bergamini, P., Bernardi, F., Bertaina, M. E., Bessin, P., Betti, L., Bettonvil, F., Bihel, D., Birnbaum, C., Blagoi, O., Blouri, E., Boaca, I., Boat, R., Bobiet, B., Bonino, R., Boros, K., Bouchet, E., Borgeot, V., Bouchez, E., Boust, D., Boudon, V., Bouman, T., Bourget, P., Brandenburg, S., Bramond, Ph., Braun, E., Bussi, A., Cacault, P., Caillier, B., Calegario, A., Camargo, J., Caminade, S., Campana, A. P. C., Campbell-Burns, P., Canal-Domingo, R., Carell, O., Carreau, S., Cascone, E., Cattaneo, C., Cauhape, P., Cavier, P., Celestin, S., Cellino, A., Champenois, M., Chennaoui Aoudjehane, H., Chevrier, S., Cholvy, P., Chomier, L., Christou, A., Cricchio, D., Coadou, P., Coccagn, J. Y., Cochard, F., Cointin, S., Colombi, E., Colque Saavedra, J. P., Corp, L., Costa, M., Costard, F., Cottier, M., Cournoyer, P., Coustal, E., Cremonese, G., Cristea, O., Cuzon, J. C., D'Agostino, G., Daiffallah, K., Du, C., Dardon, A., Dasse, T., Davadan, C., Debs, V., Defaix, J. P., Deleflie, F., D'Elia, M., De Luca, P., De Maria, P., Deverchère, P., Devillepoix, H., Dias, A., Di Dato, A., Di Luca, R., Dominici, F. M., Drouard, A., Dumont, J. L., Dupouy, P., Duvinac, L., Egal, A., Erasmus, N., Esseiva, N., Ebel, A., Eisengarten, B., Federici, F., Feral, S.,

Ferrant, G., Ferreol, E., Finitzer, P., Foucault, A., Francois, P., Frîncu, M., Froger, J. L., Gaborit, F., Gagliarducci, V., Galard, J., Gardavot, A., Garmier, M., Garnung, M., Gautier, B., Gendre, B., Gerard, D., Gerardi, A., Godet, J. P., Grandchamps, A., Grouiez, B., Groult, S., Guidetti, D., Giuli, G., Hello, Y., Henry, X., Herbreteau, G., Herpin, M., Hewins, P., Hillairet, J. J., Horak, J., Hueso, R., Huet, E., Huet, S., Hyaumé, F., Interrante, G., Is-selin, Y., Jeangeorges, Y., Janeux, P., Jeanneret, P., Jobse, K., Jouin, S., Jouvard, J. M., Joy, K., Julien, J. F., Kacerek, R., Kaire, M., Kempf, M., Koschny, D., Krier, C., Kwon, M. K., Lacassagne, L., Lachat, D., Lagain, A., Laisné, E., Lanchares, V., Laskar, J., Lazzarin, M., Leblanc, M., Lebreton, J. P., Lecomte, J., Le Dû, P., Lelong, F., Lera, S., Leoni, J. F., Le-Pichon, A., Le-Poupon, P., Leroy, A., Leto, G., Levansuu, A., Lewin, E., Lienard, A., Licchelli, D., Locatelli, H., Loehle, S., Loizeau, D., Luciani, L., Maignan, M., Manca, F., Mancuso, S., Mandon, E., Mangold, N., Mannucci, F., Maquet, L., Marant, D., Marchal, Y., Marin, J. L., Martin-Brisset, J. C., Martin, D., Mathieu, D., Maury, A., Mespoulet, N., Meyer, F., Meyer, J. Y., Meza, E., Moggi Cecchi, V., Moiroud, J. J., Millan, M., Montes-archio, M., Misiano, A., Molinari, E., Molau, S., Monari, J., Monflier, B., Monkos, A., Montemaggi, M., Monti, G., Moreau, R., Morin, J., Mourgues, R., Mousis, O., Nablanc, C., Nastasi, A., Niacsu, L., Notez, P., Ory, M., Pace, E., Paganelli, M. A., Pagola, A., Pajuelo, M., Palacián, J. F., Pallier, G., Paraschiv, P., Pardini, R., Pavone, M., Pavy, G., Payen, G., Pegoraro, A., Peña-Asensio, E., Perez, L., Pérez-Hoyos, S., Perlerin, V., Peyrot, A., Peth, F., Pic, V., Pietronave, S., Pilger, C., Piquel, M., Pisanu, T., Poppe, M., Porto, L., Prezeau, J. F., Pugno, N., Quantin, C., Quitté, G., Rambaux, N., Ravier, E., Repetti, U., Ribas, S., Richard, C., Richard, D., Rigoni, M., Rivet, J. P., Rizzi, N., Rochain, S., Rojas, J.F., Romeo, M., Rotaru, M., Rotger, M., Rougier, P., Rousselot, P., Rousset, J., Rousseu, D., Rubiera, O., Rudawska, R., Rudelle, J., Ruguet, J.P., Russo, P., Sales, S., Sauzereau, O., Salvati, F., Schieffer, M., Schreiner, D., Scribano, Y., Selvestrel, D., Serra, R., Shengold, L., Shuttleworth, A., Smareglia, R., Sohy, S., Soldi, M., Stanga, R., Steinhausser, A., Strafella, F., Sylla Mbaye, S., Smedley, A. R. D., Tagger, M., Tanga, P., Taricco, C., Teng, J. P., Tercu, J. O., Thizy, O., Thomas, J. P., Tombelli, M., Trangosi, R., Tregon, B., Trivero, P., Tukkers, A., Turcu, V., Umbriaco, G., Unda-Sanzana, E., Vairetti, R., Valenzuela, M., Valente, G., Varennes, G., Vauclair, S., Vergne, J., Verlinden, M., Vidal-Alaiz, M., Vieira-Martins, R., Viel, A., Vîntdevar, D. C., Vinogradoff, V., Volpini, P., Wendling, M., Wilhelm, P., Wohlgemuth, K., Yanguas, P., Zagarella, R. and Zollo, A. 2020, 'Fripon: a world-wide network to track incoming meteoroids', *Astronomy and Astrophysics*, vol. 644, pp. A53.

, <https://doi.org/10.1051/0004-6361/202038649>

Davis, J. 1963, 'Photoelectric meteor observations and the colour indices and visual magnitudes of meteors', *Monthly Notices of the Royal Astronomical Society*, vol. 126, pp. 445.

de Bruijn, N. 1946, 'A combinatorial problem', *Proceedings of the Section of Sciences of the Koninklijke Nederlandse Akademie van Wetenschappen te Amsterdam*, vol. 49, no. 7, pp. 758–764.

DeMeo, F. E., Binzel, R. P., Slivan, S. M. and Bus, S. J. 2009, 'An extension of the bus asteroid taxonomy into the near-infrared', *Icarus*, vol. 202, no. 1, pp. 160–180.

Devillepoix, H. A. R. (2018), Commissioning and First Science Results of the Desert Fireball Network: a Global-Scale Automated Survey for Large Meteoroid Impacts, PhD thesis, Curtin University, Perth, Western Australia. , <http://hdl.handle.net/20.500.11937/76001>

Devillepoix, H. A. R., Cupák, M., Bland, P. A., Sansom, E. K., Towner, M. C., Howie, R. M., Hartig, B. A. D., Jansen-Sturgeon, T., Shober, P. M., Anderson, S. L., Benedix, G. K., Busan, D., Sayers, R., Jenniskens, P., Albers, J., Herd, C. D. K., Hill, P. J. A., Brown, P. G., Krzeminski, Z., Osinski, G. R., Aoudjehane, H. C., Benkhaldoun, Z., Jabiri, A., Guennoun, M., Barka, A., Darhmaoui, H., Daly, L., Collins, G. S., McMullan, S., Suttle, M. D., Ireland, T., Bonning, G., Baeza, L., Alrefay, T. Y., Horner, J., Swindle, T. D., Hergenrother, C. W., Fries, M. D., Tomkins, A., Langendam, A., Rushmer, T., O'Neill, C., Janches, D., Hormaechea, J. L., Shaw, C., Young, J. S., Alexander, M., Mardon, A. D. and Tate, J. R. 2020, 'A Global Fireball Observatory', *Planetary and Space Science*, vol. 191, pp. 105036.

Devillepoix, H. A. R., Sansom, E. K., Bland, P. A., Towner, M. C., Cupák, M., Howie, R. M., Jansen-Sturgeon, T., Cox, M. A., Hartig, B. A. D., Benedix, G. K. and Paxman, J. P. 2018, 'The dingle dell meteorite: A halloween treat from the main belt', *Meteoritics and Planetary Science*, vol. 53, no. 10, pp. 2212–2227. , <https://onlinelibrary.wiley.com/doi/abs/10.1111/maps.13142>

Duda, R. O. and Hart, P. E. 1972, 'Use of the hough transformation to detect lines and curves in pictures', *Commun. ACM*, vol. 15, no. 1, pp. 11–15. , <https://doi.org/10.1145/361237.361242>

Dworkin, J. P. and Osiris-Rex Team, 2017, Status of the osiris-rex sample return mission, in 'XVIIIth International Conference on the Origin of Life', vol. 1967 of *LPI Contributions*, pp. 4095.

Eisenstein, D. J., Annis, J., Gunn, J. E., Szalay, A. S., Connolly, A. J., Nichol, R. C., Bahcall, N. A., Bernardi, M., Burles, S., Castander, F. J., Fukugita, M., Hogg, D. W., Ivezić, Ž., Knapp, G. R., Lupton, R. H., Narayanan, V., Postman, M., Reichart, D. E., Richmond, M., Schneider, D. P., Schlegel, D. J., Strauss, M. A., SubbaRao, M., Tucker, D. L., Berk, D. V., Vogeley, M. S., Weinberg, D. H. and Yanny, B. 2001, 'Spectroscopic target selection for the sloan digital sky survey: The luminous red galaxy sample', *The Astronomical Journal*, vol. 122, no. 5, pp. 2267–2280. , <https://doi.org/10.1086/323717>

F1, I. C., 2017, 'Definitions of terms in meteor astronomy'. , https://www.iau.org/science/scientific_bodies/commissions/F1/

Flye Sainte-Marie, C. 1894, 'Question nr. 48', *L'Intermédiaire Math*, vol. 1, pp. 19–20.

Frohn, O., 2017, 'Logarithmic overview of the universe'. , <https://armchairastronautics.blogspot.com/2017/03/logscale-universe.html>

Ganapathy, R. and Brownlee, D. E. 1979, 'Interplanetary dust: Trace element analysis of individual particles by neutron activation', *Science*, vol. 206, no. 4422, pp. 1075–1077.

Garcia, R. F., Daubar, I. J., Beucler, É., Posiolova, L. V., Collins, G. S., Lognonné, P., Rolland, L., Xu, Z., Wójcicka, N., Spiga, A., Fernando, B., Speth, G., Martire, L., Rajšić, A., Miljković, K., Sansom, E. K., Charalambous, C., Ceylan, S., Menina, S., Margerin, L., Lapeyre, R., Neidhart, T., Teanby, N. A., Schmerr, N. C., Banerdt, W. B., Froment, M., Clinton, J. F., Karatekin, O., Stähler, S. C., Dahmen, N. L., Durán, C., Horleston, A., Kawamura, T., Plasman, M., Zenhäusern, G., Giardini, D., Panning, M., Malin, M. and Banerdt, W. B. 2022, 'Newly formed craters on Mars located using seismic and acoustic wave data from InSight', *Nature Geoscience*, vol. 15, pp. 774–780.

Grossman, J., 2005, 'Meteoritical bulletin database'. , <https://www.lpi.usra.edu/meteor/>

Guo, H. and Gu, M. 2014, 'The optical variability of sdss quasars from multi-epoch spectroscopy. i. results from 60 quasars with \geq six-epoch spectra', *The Astrophysical Journal*, vol. 792.

- Hajduková, M. 1967, 'The colour index of visual meteors', *Bulletin of the Astronomical Institutes of Czechoslovakia*, vol. 18, pp. 187.
- Hajdukova, M. 1974, 'The Dependence of the Colour Index of Meteors on their Velocity', *Bulletin of the Astronomical Institutes of Czechoslovakia*, vol. 25, pp. 365.
- Hobbs, G., Lyne, A. G., Kramer, M., Martin, C. E. and Jordan, C. 2004, 'Long-term timing observations of 374 pulsars', *Monthly Notices of the Royal Astronomical Society*, vol. 353, no. 4, pp. 1311–1344. , <https://doi.org/10.1111/j.1365-2966.2004.08157.x>
- Horner, J., Kane, S. R., Marshall, J. P., Dalba, P. A., Holt, T. R., Wood, J., Maynard-Casely, H. E., Wittenmyer, R., Lykawka, P. S., Hill, M., Salmeron, R., Bailey, J., Löhne, T., Agnew, M., Carter, B. D. and Tylor, C. C. E. 2020, 'Solar system physics for exoplanet research', *Publications of the Astronomical Society of the Pacific*, vol. 132, no. 1016, pp. 102001.
- Howie, R. M., Paxman, J., Bland, P. A., Towner, M. C., Cupak, M., Sansom, E. K. and Devillepoix, H. A. R. 2017, 'How to build a continental scale fireball camera network', *Experimental Astronomy*, vol. 43, no. 3, pp. 237–266.
- Howie, R. M., Paxman, J., Bland, P. A., Towner, M. C., Sansom, E. K. and Devillepoix, H. A. R. 2017, 'Submillisecond fireball timing using de Bruijn timecodes', *Meteoritics and Planetary Science*, vol. 52, no. 8, pp. 1669–1682.
- Hutchison, R. 2007, *Meteorites: A Petrologic, Chemical and Isotopic Synthesis*, Cambridge University Press, Great Britain.
- Jacchia, L. G. 1957, 'On the "color index" of meteors', *Astronomical Journal*, vol. 62, pp. 358.
- Jenniskens, P. 2006, *Meteor Showers and their Parent Comets*, Cambridge University Press.
- Jenniskens, P. and Stenbaek-Nielsen, H. C. 2004, 'Meteor Wake in High Frame-Rate Images-Implications for the Chemistry of Ablated Organic Compounds', *Astrobiology*, vol. 4, no. 1, pp. 95–108.
- Jones, R. L., Jurić, M. and Ivezić, Ž., 2016, Asteroid Discovery and Characterization with the Large Synoptic Survey Telescope, in S. R. Chesley, A. Morbidelli, R. Jedicke and D. Farnocchia, eds, 'Asteroids: New Observations, New Models', vol. 318, pp. 282–292.

- Jr., H. Y. M. and Treiman, A. H. (2018), *Chapter 6. MARTIAN METEORITES*, De Gruyter, pp. 953–1006. , <https://doi.org/10.1515/9781501508806-021>
- Kalmbach, J. B., VanderPlas, J. T. and Connolly, A. J. 2020, ‘Applying Information Theory to Design Optimal Filters for Photometric Redshifts’, *The Astrophysical Journal*, vol. 890, no. 1, pp. 74.
- Krot, A., Keil, K., Goodrich, C., Scott, E. and Weisberg, M. 2013, ‘Classification of meteorites and their genetic relationships’, *Meteorites and Cosmochemical Processes: Treatise on Geochemistry*, vol. 1, pp. 1–63.
- Lee, S., 2020, ‘Lines detection with hough transform’. , <https://towardsdatascience.com/lines-detection-with-hough-transform-84020b3b1549>
- Love, S. G. and Brownlee, D. E. 1993, ‘A direct measurement of the terrestrial mass accretion rate of cosmic dust’, *Science*, vol. 262, no. 5133, pp. 550–553. , <https://www.science.org/doi/abs/10.1126/science.262.5133.550>
- Lykawka, P. S. and Ito, T. 2023, ‘Is There an Earth-like Planet in the Distant Kuiper Belt?’, *Astronomical Journal*, vol. 166, no. 3, pp. 118.
- McCord, T. B., Adams, J. B. and Johnson, T. V. 1970, ‘Asteroid vesta: Spectral reflectivity and compositional implications’, *Science*, vol. 168, no. 3938, pp. 1445–1447. , <https://www.science.org/doi/abs/10.1126/science.168.3938.1445>
- McNutt, R., Gruntman, M., Krimigis, S., Roelof, E., Brandt, P., Mandt, K., Vernon, S., Paul, M. and Stough, R., 2020, Interstellar probe: The next step, *in* ‘EGU General Assembly Conference Abstracts’, EGU General Assembly Conference Abstracts, pp. 6119.
- McSween, H. Y., J. 2001, ‘The rocks of mars, from far and near’, *Meteoritics and Planetary Science Supplement*, vol. 36, pp. A129.
- Meier, M. M. M., 2017, ‘Meteorite orbits .info’. , <https://www.meteoriteorbits.info/>
- Mendis, D. A. and Marconi, M. L. 1986, ‘A Note on the Total Mass of Comets in the Solar System’, *Earth Moon and Planets*, vol. 36, no. 2, pp. 187–190.

- Millman, P. M. 1937, 'An analysis of meteor spectra', *Annals of Harvard College Observatory*, vol. 82, pp. 113–147.
- Mittlefehldt, D., McCoy, T., Goodrich, C. and Kracher, A. (2019), *Non-chondritic meteorites from asteroidal bodies.* , https://www.researchgate.net/publication/331148298_Non-chondritic_meteorites_from_asteroidal_bodies
- Mittlefehldt, D. W. 2003, 'Achondrites', *Treatise on Geochemistry*, vol. 1, pp. 711.
- Moorhead, A. V. and Kingery, A. 2020, 'Does a meteor's "color" reflect its spectral classification?', *WGN, Journal of the International Meteor Organization*, vol. 48, no. 6, pp. 193–198.
- Morbidelli, A. 2005, 'Origin and Dynamical Evolution of Comets and their Reservoirs', *arXiv e-prints*, vol. , pp. astro-ph/0512256.
- Nakamura, T., Noguchi, T., Tanaka, M., Zolensky, M. E., Kimura, M., Tsuchiyama, A., Nakato, A., Ogami, T., Ishida, H., Uesugi, M., Yada, T., Shirai, K., Fujimura, A., Okazaki, R., Sandford, S. A., Ishibashi, Y., Abe, M., Okada, T., Ueno, M., Mukai, T., Yoshikawa, M. and Kawaguchi, J. 2011, 'Itokawa dust particles: A direct link between s-type asteroids and ordinary chondrites', *Science*, vol. 333, no. 6046, pp. 1113.
- NASA, 1981, 'Mission operation report: Voyager mission success assessment', NASA STI/Recon Technical Report N.
- Nyquist, L. E., Bogard, D. D., Shih, C. Y., Greshake, A., Stöffler, D. and Eugster, O. 2001, 'Ages and geologic histories of martian meteorites', *Space Science Reviews*, vol. 96, pp. 105–164.
- Osinski, G. R., Cockell, C. S., Pontefract, A. and Sapers, H. M. 2020, 'The Role of Meteorite Impacts in the Origin of Life', *Astrobiology*, vol. 20, no. 9, pp. 1121–1149.
- Otsu, N. 1979, 'A threshold selection method from gray-level histograms', *IEEE Transactions on Systems, Man, and Cybernetics*, vol. 9, no. 1, pp. 62–66.
- Papike, J. J., ed. 2018, *Planetary Materials*, De Gruyter. , <https://doi.org/10.1515/9781501508806>

Papike, J. J., Ryder, G. and Shearer, C. K. (2018), *Chapter 5. LUNAR SAMPLES*, De Gruyter, pp. 719–952. , <https://doi.org/10.1515/9781501508806-020>

Penzias, A. A. and Wilson, R. W. 1965, 'A measurement of excess antenna temperature at 4080 mc/s.', *The Astrophysical Journal*, vol. 142, pp. 419–421.

Plane, J. M. C. 2012, 'Cosmic dust in the earth's atmosphere', *Chemical Society Reviews*, vol. 41, pp. 6507–6518.

Redfern, G. I. (2020), *Asteroids, Comets, Meteors, Fireballs, Bolides, and Meteor Showers*, Springer International Publishing, Cham, pp. 311–328. , <https://doi.org/10.1007/978-3-030-45943-7-17>

Richardson, J., 2021, 'Fireball faqs' . , <https://www.amsmeteors.org/fireballs/faqf/>

Rigby, J., Perrin, M., McElwain, M., Kimble, R., Friedman, S., Lallo, M., Doyon, R., Feinberg, L., Ferruit, P., Glasse, A., Rieke, M., Rieke, G., Wright, G., Willott, C., Colon, K., Milam, S., Neff, S., Stark, C., Valenti, J., Abell, J., Abney, F., Abul-Huda, Y., Acton, D. S., Adams, E., Adler, D., Aguilar, J., Ahmed, N., Albert, L., Alberts, S., Aldridge, D., Allen, M., Altenburg, M., Alvarez Marquez, J., Alves de Oliveira, C., Andersen, G., Anderson, H., Anderson, S., Argyriou, I., Armstrong, A., Arribas, S., Artigau, E., Arvai, A., Atkinson, C., Bacon, G., Bair, T., Banks, K., Barrientes, J., Barringer, B., Bartosik, P., Bast, W., Baudoz, P., Beatty, T., Bechtold, K., Beck, T., Bergeron, E., Bergkoetter, M., Bhatawdekar, R., Birkmann, S., Blazek, R., Blome, C., Boccaletti, A., Boeker, T., Boia, J., Bonaventura, N., Bond, N., Bosley, K., Boucarut, R., Bourque, M., Bouwman, J., Bower, G., Bowers, C., Boyer, M., Bradley, L., Brady, G., Braun, H., Breda, D., Bresnahan, P., Bright, S., Britt, C., Bromenschenkel, A., Brooks, B., Brooks, K., Brown, B., Brown, M., Brown, P., Bunker, A., Burger, M., Bushouse, H., Cale, S., Cameron, A., Cameron, P., Canipe, A., Caplinger, J., Caputo, F., Cara, M., Carey, L., Carniani, S., Carrasquilla, M., Carruthers, M., Case, M., Catherine, R., Chance, D., Chapman, G., Charlot, S., Charlow, B., Chayer, P., Chen, B., Cherinka, B., Chichester, S., Chilton, Z., Chonis, T., Clampin, M., Clark, C., Clark, K., Coe, D., Coleman, B., Comber, B., Comeau, T., Connolly, D., Cooper, J., Cooper, R., Coppock, E., Correnti, M., Cossou, C., Coulais, A., Coyle, L., Cracraft, M., Curti, M., Cuturic, S., Davis, K., Davis, M., Dean, B., DeLisa, A., deMeester, W., Dencheva, N., Dencheva, N., DePasquale, J., Deschenes, J., Hunor Detre, Ö., Diaz, R., Dicken, D.,

DiFelice, A., Dillman, M., Dixon, W., Doggett, J., Donaldson, T., Douglas, R., DuPrie, K., Dupuis, J., Durning, J., Easmin, N., Eck, W., Edeani, C., Egami, E., Ehrenwinkler, R., Eisenhamer, J., Eisenhower, M., Elie, M., Elliott, J., Elliott, K., Ellis, T., Engesser, M., Espinoza, N., Etienne, O., Etxaluze, M., Falini, P., Feeney, M., Ferry, M., Filippazzo, J., Fincham, B., Fix, M., Flagey, N., Florian, M., Flynn, J., Fontanella, E., Ford, T., Forshay, P., Fox, O., Franz, D., Fu, H., Fullerton, A., Galkin, S., Galyer, A., Garcia Marin, M., Gardner, J., Gardner, L., Garland, D., Garrett, B., Gasman, D., Gaspar, A., Gaudreau, D., Gauthier, P., Geers, V., Geithner, P., Gennaro, M., Giardino, G., Girard, J., Giuliano, M., Glassmire, K., Glauser, A., Glazer, S., Godfrey, J., Golimowski, D., Gollnitz, D., Gong, F., Gonzaga, S., Gordon, M., Gordon, K., Goudfrooij, P., Greene, T., Greenhouse, M., Grimaldi, S., Groebner, A., Grundy, T., Guillard, P., Gutman, I., Ha, K. Q., Haderlein, P., Hagedorn, A., Hainline, K., Haley, C., Hami, M., Hamilton, F., Hammel, H., Hansen, C., Harkins, T., Harr, M., Hart, J., Hart, Q., Hartig, G., Hashimoto, R., Haskins, S., Hathaway, W., Havey, K., Hayden, B., Hecht, K., Heller-Boyer, C., Henriques, C., Henry, A., Hermann, K., Hernandez, S., Hesman, B., Hicks, B., Hilbert, B., Hines, D., Hoffman, M., Holfeltz, S., Holler, B. J., Hoppa, J., Hott, K., Howard, J., Howard, R., Hunter, A., Hunter, D., Hurst, B., Husemann, B., Hustak, L., Ilinca Ignat, L., Illingworth, G., Irish, S., Jackson, W., Jahromi, A., Jakobsen, P., James, L., James, B., Januszewski, W., Jenkins, A., Jirdeh, H., Johnson, P., Johnson, T., Jones, V., Jones, R., Jones, D., Jones, O., Jordan, I., Jordan, M., Jurczyk, S., Jurling, A., Kaleida, C., Kalmanson, P., Kammerer, J., Kang, H., Kao, S.-H., Karakla, D., Kavanagh, P., Kelly, D., Kendrew, S., Kennedy, H., Kenny, D., Keski-kuha, R., Keyes, C., Kidwell, R., Kinzel, W., Kirk, J., Kirkpatrick, M., Kirshenblat, D., Klaassen, P., Knapp, B., Knight, J. S., Knollenberg, P., Koehler, R., Koekemoer, A., Kovacs, A., Kulp, T., Kumari, N., Kyprianou, M., La Massa, S., Labador, A., Labiano Ortega, A., Lagage, P.-O., Lajoie, C.-P., Lallo, M., Lam, M., Lamb, T., Lambros, S., Lampenfield, R., Langston, J., Larson, K., Law, D., Lawrence, J., Lee, D., Leisenring, J., Lepo, K., Leveille, M., Levenson, N., Levine, M., Levy, Z., Lewis, D., Lewis, H., Libralato, M., Lightsey, P., Link, M., Liu, L., Lo, A., Lockwood, A., Logue, R., Long, C., Long, D., Loomis, C., Lopez-Caniego, M., Alvarez, J. L., Love-Pruitt, J., Lucy, A., Luetzgendorf, N., Maghami, P., Maiolino, R., Major, M., Malla, S., Malumuth, E., Manjavacas, E., Mannfolk, C., Marrione, A., Marston, A., Martel, A., Maschmann, M., Masci, G., Masciarelli, M., Maszkiewicz, M., Mather, J., McKenzie, K., McLean, B., McMaster, M., Melbourne, K., Meléndez, M., Menzel, M., Merz, K., Meyett, M., Meza, L., Miskey, C., Misselt, K., Moller, C., Morrison, J., Morse,

E., Moseley, H., Mosier, G., Mountain, M., Mueckay, J., Mueller, M., Mullally, S., Murphy, J., Murray, K., Murray, C., Mustelier, D., Muzerolle, J., Mycroft, M., Myers, R., Myrick, K., Nanavati, S., Nance, E., Nayak, O., Naylor, B., Nelan, E., Nickson, B., Nielson, A., Nieto-Santisteban, M., Nikolov, N., Noriega-Crespo, A., O'Shaughnessy, B., O'Sullivan, B., Ochs, W., Ogle, P., Oleszczuk, B., Olmsted, J., Osborne, S., Ottens, R., Owens, B., Pacifici, C., Pagan, A., Page, J., Park, S., Parrish, K., Patapis, P., Paul, L., Pauly, T., Pavlovsky, C., Pedder, A., Peek, M., Pena-Guerrero, M., Pennanen, K., Perez, Y., Perna, M., Perriello, B., Phillips, K., Pietraszkiewicz, M., Pinaud, J.-P., Pirzkal, N., Pitman, J., Piwowar, A., Platais, V., Player, D., Plesha, R., Pollizi, J., Polster, E., Pontoppidan, K., Porterfield, B., Proffitt, C., Pueyo, L., Pulliam, C., Quirt, B., Quispe Neira, I., Ramos Alarcon, R., Ramsay, L., Rapp, G., Rapp, R., Rauscher, B., Ravindranath, S., Rawle, T., Regan, M., Reichard, T. A., Reis, C., Ressler, M. E., Rest, A., Reynolds, P., Rhue, T., Richon, K., Rickman, E., Ridgeway, M., Ritchie, C., Rix, H.-W., Robberto, M., Robinson, G., Robinson, M., Robinson, O., Rock, F., Rodriguez, D., Rodriguez Del Pino, B., Roellig, T., Rohrbach, S., Roman, A., Romelfanger, F., Rose, P., Roteliuk, A., Roth, M., Rothwell, B., Rowlands, N., Roy, A., Royer, P., Royle, P., Rui, C., Rumler, P., Runnels, J., Russ, M., Rustamkulov, Z., Ryden, G., Ryer, H., Sabata, M., Sabatke, D., Sabbi, E., Samuelson, B., Sapp, B., Sappington, B., Sargent, B., Sauer, A., Scheithauer, S., Schlawin, E., Schlitz, J., Schmitz, T., Schneider, A., Schreiber, J., Schulze, V., Schwab, R., Scott, J., Sembach, K., Shanahan, C., Shaughnessy, B., Shaw, R., Shawger, N., Shay, C., Sheehan, E., Shen, S., Sherman, A., Shiao, B., Shih, H.-Y., Shivaie, I., Sienkiewicz, M., Sing, D., Sirianni, M., Sivaramakrishnan, A., Skipper, J., Sloan, G., Slocum, C., Slowinski, S., Smith, E., Smith, E., Smith, D., Smith, C., Snyder, G., Soh, W., Sohn, T., Soto, C., Spencer, R., Stallcup, S., Stansberry, J., Starr, C., Starr, E., Stewart, A., Stiavelli, M., Straughn, A., Strickland, D., Stys, J., Summers, F., Sun, F., Sunnquist, B., Swade, D., Swam, M., Swaters, R., Swoish, R., Taylor, J. M., Taylor, R., Te Plate, M., Tea, M., Teague, K., Telfer, R., Temim, T., Thatte, D., Thompson, C., Thompson, L., Thomson, S., Tikkanen, T., Tippet, W., Todd, C., Toolan, S., Tran, H., Trejo, E., Truong, J., Tsukamoto, C., Tustain, S., Tyra, H., Ubeda, L., Underwood, K., Uzzo, M., Van Campen, J., Vandal, T., Vandenbussche, B., Vila, B., Volk, K., Wahlgren, G., Waldman, M., Walker, C., Wander, M., Warfield, C., Warner, G., Wasiak, M., Watkins, M., Weaver, A., Weilert, M., Weiser, N., Weiss, B., Weissman, S., Welty, A., West, G., Wheate, L., Wheatley, E., Wheeler, T., White, R., Whiteaker, K., Whitehouse, P., Whiteleather, J., Whitman, W., Williams, C., Willmer, C., Willoughby, S., Wilson, A., Wirth, G., Wislowski, E., Wolf, E., Wolfe, D.,

- Wolff, S., Workman, B., Wright, R., Wu, C., Wu, R., Wymer, K., Yates, K., Yeager, C., Yeates, J., Yerger, E., Yoon, J., Young, A., Yu, S., Zak, D., Zeidler, P., Zhou, J., Zielinski, T., Zincke, C. and Zonak, S. 2022, 'Characterization of JWST science performance from commissioning', *arXiv e-prints*, vol. , pp. arXiv:2207.05632.
- Sansom, E. K. (2016), Tracking Meteoroids in the Atmosphere: Fireball Trajectory Analysis, PhD thesis, Curtin University, Perth, Western Australia. , <https://espace.curtin.edu.au/handle/20.500.11937/55061>
- Sansom, E. K., Bland, P., Paxman, J. and Towner, M. 2015, 'A novel approach to fireball modeling: The observable and the calculated', *Meteoritics and Planetary Science*, vol. 50, no. 8, pp. 1423–1435. , <https://onlinelibrary.wiley.com/doi/abs/10.1111/maps.12478>
- Sansom, E. K., Rutten, M. G. and Bland, P. A. 2017, 'Analyzing meteoroid flights using particle filters', *The Astronomical Journal*, vol. 153, no. 2, pp. 87. , <http://dx.doi.org/10.3847/1538-3881/153/2/87>
- Siraj, A. and Loeb, A. 2020, 'Searching for black holes in the outer solar system with lsst', *The Astrophysical Journal Letters*, vol. 898, no. 1, pp. L4.
- Siraj, A. and Loeb, A. 2021, 'The new astronomical frontier of interstellar objects', *arXiv e-prints*, vol. , pp. arXiv:2111.05516.
- Snead, L. L., Hoelzer, D. T., Rieth, M. and Nemith, A. A., 2019, Chapter 13 - refractory alloys: Vanadium, niobium, molybdenum, tungsten, *in* G. R. Odette and S. J. Zinkle, eds, 'Structural Alloys for Nuclear Energy Applications', Elsevier, Boston, pp. 585–640.
- Sugita, S., Honda, R., Morota, T., Kameda, S., Tatsumi, E., Tachibana, S., Kitazato, K., Okada, T., Namiki, N., Arakawa, M., Michel, P., Domingue, D., Tanaka, S., Yoshikawa, M., Watanabe, S.-i. and Tsuda, Y., 2020, Mission status of hayabus2, science highlights, and outlook for sample analyses, *in* 'European Planetary Science Congress', pp. EPSC2020–995.
- Tholen, D.J. (1984), Asteroid Taxonomy From Cluster Analysis of Photometry, PhD thesis, The University of Arizona, Arizona. , <https://repository.arizona.edu/handle/10150/187738>
- Thompson Sr., S. B. 2012, 'The night the stars fell', *Pieces of Our Past, Dublin Laurens County Georgia Blogspot*, vol. . , <http://dublinlaurenscountygeorgia.blogspot.com/2012/11/the-night-stars-fell.html>

Todd, C. J., Sansom, E. K., Devillepoix, H. A. R., Horner, J., Towner, M. C., Cupák, M., Wright, D. and Carter, B. (2023), Colour analysis of meteors using the desert fireball network. Pending final edits, all result presented in the paper are unchanged, only language is changed.

Tomko, D. and Neslušan, L. 2023, 'Prediction of the collisions of meteoroids originating in comet 21P/Giacobini-Zinner with the Mercury, Venus, and Mars', *Icarus*, vol. 405, pp. 115694.

Trigo-Rodríguez, J. M., 2014, Meteor emission spectroscopy: clues on the delivery of primitive materials from cometary meteoroids, in T. J. Jopek, F. J. M. Rietmeijer, J. Watanabe and I. P. Williams, eds, 'Meteoroids 2013', pp. 105–116.

Trigo-Rodríguez, J. M. and Llorca, J. 2007, 'On the sodium overabundance in cometary meteoroids', *Advances in Space Research*, vol. 39, no. 4, pp. 517–525.

Trujillo, C. A. and Sheppard, S. S. 2014, 'A Sedna-like body with a perihelion of 80 astronomical units', *Nature*, vol. 507, no. 7493, pp. 471–474.

Čapek, D. and Borovička, J. 2009, 'Quantitative model of the release of sodium from meteoroids in the vicinity of the Sun: Application to Geminids', *Icarus*, vol. 202, no. 2, pp. 361–370.

Vernazza, P., Binzel, R. P., Thomas, C. A., DeMeo, F. E., Bus, S. J., Rivkin, A. S. and Tokunaga, A. T. 2008, 'Compositional differences between meteorites and near-earth asteroids', *Nature*, vol. 454, no. 7206, pp. 858–860.

Vladimirovna Pitjeva, E. and Petrovich Pitjev, N., 2015, Masses of asteroids and the total mass of the main asteroid belt, in 'IAU General Assembly', vol. 29, pp. 2256597.

Vojáček, V., Borovička, J., Koten, P., Spurný, P. and Štork, R. 2015a, 'Catalogue of representative meteor spectra', *Astronomy and Astrophysics*, vol. 580, pp. A67.

Vojáček, V., Borovička, J., Koten, P., Spurný, P. and Štork, R. 2015b, 'Catalogue of representative meteor spectra', *Astronomy and Astrophysics*, vol. 580, pp. A67.

Volk, K. and Malhotra, R. 2017, 'The Curiously Warped Mean Plane of the Kuiper Belt', *Astronomical Journal*, vol. 154, no. 2, pp. 62.

Weisberg, M. K., McCoy, T. J. and Krot, A. N. (2006), *Systematics and Evaluation of Meteorite Classification*, pp. 19.

Whipple, F. L. 1938, 'Photographic meteor studies, i', *Proceedings of the American Philosophical Society*, vol. 79, no. 4, pp. 499–548. , <http://www.jstor.org/stable/984939>

Whipple, F. L. and El-Din Hamid, S. 1952, 'On the Origin of the Taurid Meteor Streams', *Helwan Institute of Astronomy and Geophysics Bulletins*, vol. 41, pp. 3–30.

Wikipedia/Tobias1984, 2012, 'Meteorite classification, based on weisberg, mccoys and krot 2006', https://commons.wikimedia.org/wiki/File:Meteorite_Classification_after_Weissberg_McCoy_Krot_2006.

Yeomans, D. K. 1981, 'Comet Tempel-Tuttle and the Leonid meteors', *Icarus*, vol. 47, no. 3, pp. 492–499.

Yeomans, D. K., Yau, K. K. and Weissman, P. R. 1996, 'The Impending Appearance of Comet Tempel-Tuttle and the Leonid Meteors', *Icarus*, vol. 124, no. 2, pp. 407–413.

Yoshikawa, M., Kawaguchi, J., Fujiwara, A. and Tsuchiyama, A., 2021, Chapter 6 - the hayabusa mission, *in* A. Longobardo, ed., 'Sample Return Missions', Elsevier, pp. 123–146.

This page intentionally left blank.